Applications of the improved Jørgensen equation for tetrad effect of REE^{3+} to the REE patterns of kimuraite and lanthanite, and to the REE distribution pattern between kimuraite and lanthanite

Wenfang Jiao

Department of Earth and Planetary Sciences,

Graduate School of Environmental Studies,

Nagoya University

Contents

1. Introductions to tetrad effect

1.1 What is tetrad effect?

Actually, most colleagues may probably have little knowledge about what tetrad effect is, since there is only a small amount of publications concerning tetrad effect at present. But when it comes to the lanthanides (Ln, or REE), a particular group composed by fifteen metal elements that have received enormous attention in many fields, every colleague is supposed to be quite familiar with them. As a matter of fact, tetrad effect is closely related with the lanthanides, and it is a term adopted exactly to describe a special property exhibited by the lanthanide ions with +3 oxidation states [Ln^{3+}, or REE^{3+}]. Therefore, the lanthanides will become one of the main targets in our study.

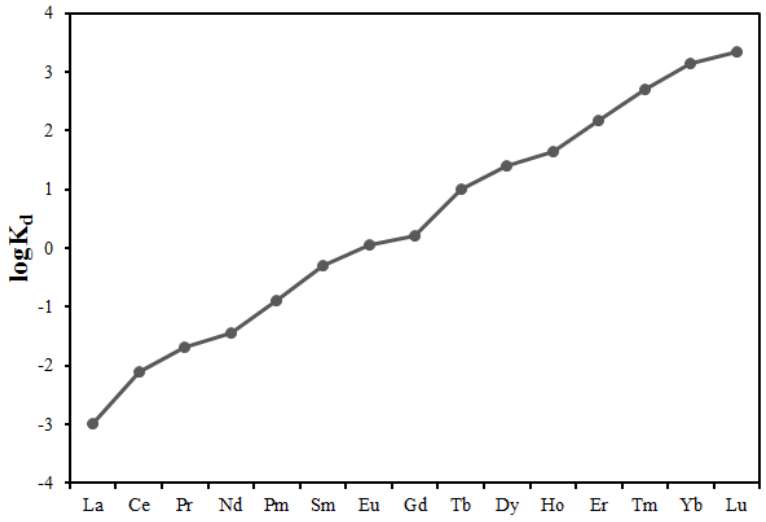

Figure 1.1 The logK_d distribution pattern of Ln^{3+} in the liquid-liquid extraction experiment between 0.3M H[DOP](benzene) and 0.05M HCl (Peppard et al., 1969).

Tetrad effect began to show up in the late 1960s. Peppard et al. (1969) performed a liquid-liquid extraction experiment of Ln^{3+}, in which the lanthanide ions were allowed to distribute at equilibrium between two immiscible liquid phases. When the logK_d (K_d is the partition coefficient of Ln^{3+}) is plotted against the atomic number Z of the lanthanides, four smooth curves can be discerned (Fig. 1.1), and each curve consists of four lanthanides, with Gd being the common point of the second and the third curves. In other words, the lanthanide series is divided into four subgroups, La-Ce-Pr-Nd, (Pm)-Sm-Eu-Gd, Gd-Tb-Dy-Ho, Er-Tm-Yb-Lu, with each group

corresponding to one curve. Four curves yield three intersection points. From the perspective of the electron configurations of Ln^{3+}, these points are correspondent with the 1/4 filled 4f subshell at between Nd^{3+} and Pm^{3+}, the half-filled 4f subshell at Gd^{3+}, and the 3/4 filled 4f subshell at between Ho^{3+} and Er^{3+} (Peppard et al., 1969).

Interestingly, Peppard and co-workers seemed unaware of the similar result having already been reported by Fidelis and Siekierski (1966), and their paper was quickly followed by a claim made by Fidelis et al. (1971), arguing that it was the latter group that first recognize the existence of tetrad effect, and that Peppard and his fellows did nothing new rather than gave a name to the distribution pattern.

Briefly, tetrad effect is an irregular and peculiar distribution pattern of the lanthanides, which is also called tetrad pattern. In addition, besides tetrad effect, other terms, like zig-zag pattern and double-double pattern, were once used in some papers to describe this special property of the lanthanides.

In the following sections, we will mainly deal with one important question. That is why the lanthanide ions display a tetrad pattern, instead of a smooth pattern which seems more acceptable as far as their radii and similar electronegativities are considered. First, we would like to provide some basic introductions about the electronic configurations of the lanthanides and their 4f electrons, as we have related the tetrad effect to the 4f subshell of Ln^{3+}. Then, we will look into the relationship between 4f electrons and the tetrad effect.

1.2 Interpretation of tetrad effect

As we know, both crystal field effect and inter-electron repulsion within either d or f sub-shell produce irregularities in the chemistry of transition elements. For the lanthanides, the 4f subshell locates inside the filled 5s and 5p subshells, and the 4f electrons are kept from participating significantly in bonding, thus, the crystal field effect is very small. Contrarily, irregularities due to inter-electron repulsion within 4f subshell are fairly obvious for the lanthanide series. As a matter of fact, the tetrad effect has been proved to be a result of the inter-electron repulsion within 4f subshell.

1.2.1 Electron configurations of the lanthanides

In chemistry, the lanthanides are a special group made up of fifteen elements, starting from lanthanum (Z=57) and continuing up to the lutetium (Z=71). All these elements resemble to each other very closely due to the same number of electrons in

the outermost shell. The most important feature of the lanthanides is the electron being added into the incomplete 4f subshell, which entitles them the inner transition elements, or inner transition metals. For the sake of making a better understanding of the lanthanides, we would better start from their electronic configurations (Table 1.1).

	Eectronic configurations of Ln (g) and Ln^{3+} (g)		ionic radii (pm)
	Ln	Ln^{3+}	Ln^{3+}
La	$[Xe]5d^16s^2$	[Xe]	103.2
Ce	$[Xe]4f^15d^16s^2$	$[Xe]4f^1$	101.0
Pr	$[Xe]4f^36s^2$	$[Xe]4f^2$	99.0
Nd	$[Xe]4f^46s^2$	$[Xe]4f^3$	98.3
Pm	$[Xe]4f^56s^2$	$[Xe]4f^4$	97.0
Sm	$[Xe]4f^66s^2$	$[Xe]4f^5$	95.8
Eu	$[Xe]4f^76s^2$	$[Xe]4f^6$	94.7
Gd	$[Xe]4f^75d^16s^2$	$[Xe]4f^7$	93.8
Tb	$[Xe]4f^96s^2$	$[Xe]4f^8$	92.3
Dy	$[Xe]4f^{10}6s^2$	$[Xe]4f^9$	91.2
Ho	$[Xe]4f^{11}6s^2$	$[Xe]4f^{10}$	90.1
Er	$[Xe]4f^{12}6s^2$	$[Xe]4f^{11}$	89.0
Tm	$[Xe]4f^{13}6s^2$	$[Xe]4f^{12}$	88.0
Yb	$[Xe]4f^{14}6s^2$	$[Xe]4f^{13}$	86.8
Lu	$[Xe]4f^{14}5d^16s^2$	$[Xe]4f^{14}$	86.1

([Xe]:$1s^22s^22p^63s^23p^63d^{10}4s^24p^64d^{10}5s^25p^6$)

Table 1.1 Electronic configurations of Ln (g) and Ln^{3+}(g), together with ionic radii for Ln^{3+} (Greenwood and Earnshaw, 1997).

For convenience, the symbol of [Xe] is employed here to represent the common electronic configuration between xenon and the lanthanides. For the lanthanide atoms, all elements have 6s subshell fully occupied, but variable occupancy of 4f and 5d sub-shells. Because of the insufficient contraction of 4f subshell, the 5d subshell of La is lower in energy level than 4f, and the first electron is arranged in 5d to keep the atom as a whole at the most stable state (Cotton, 2006). However, as the 4f contracts rapidly, the stability of 4f grows, and Ce has the second electron added into 4f

subshell, and the addition of electrons into 4f continues from Pr to Eu, which share an electron configuration of $[Xe]4f^q6s^2$ (q=3-7). When the 4f sub-shell reaches its half-filled state at Eu (q=7), 4f gains an extra stability, and as a result, the next electron is assigned in the 5d subshell of Gd. From Tb having the electron configuration of $[Xe]4f^96s^2$, the earlier trend repeats until 4f gets fully filled at Yb (q=14), and consequently, the last lanthanide Lu has to place an electron into its 5d subshell. Because of the poor ability of 4f electrons to screen the outer orbitals from the effective nuclear charge, the atomic radius decreases from La to Lu, with exceptions of Eu and Yb.

(kJ/mole)	I_1	I_2	I_3	I_4	$I_1+I_2+I_3$
La	538	1067	1850	4819	3455
Ce	527	1047	1949	3547	3523
Pr	523	1018	2086	371	3627
Nd	529	1035	2130	3899	3694
Pm	536	1052	2150	3970	3738
Sm	543	1068	2260	3990	3871
Eu	546	1085	2404	4110	4035
Gd	593	1167	1990	4250	3750
Tb	564	1112	2114	3839	3790
Dy	572	1126	2200	4001	3898
Ho	581	1139	2204	4110	3924
Er	589	1151	2194	4115	3934
Tm	597	1163	2285	4119	4045
Yb	603	1176	2415	4220	4194
Lu	523	1340	2033	4360	3896

Table 1.2 The first, the second, the third and the forth ionization energy for lanthanides (Cotton, 2006).

The lanthanides are apt to lose three electrons to form Ln^{3+} ions, and the ionization energies needed are listed in Table 1.2. In contrast to the irregularities in the electronic configurations for lanthanide atoms, both the number of 4f electrons and the ionic radii of lanthanide ions increase orderly across the entire series, and the electronic configurations of Ln^{3+} ions can be written as $[Xe]4f^q$ (q=0-14). The half-filled 4f subshell appears at Gd^{3+}, and the fully filled 4f subshell appears at Lu^{3+}. In addition to the primary +3 oxidation state, Ce^{3+} can easily lose its forth electron to form Ce^{4+} with the stable electronic configuration like xenon, whereas Eu^{2+} is reluctant to lose

its third electron, in order to keep the half-filled subshell. Since Ce and Eu are more sensitive to the redox environment, they can be easily separated from other lanthanides. As a matter of fact, the tetrad effect is an essential property of the Ln^{3+} ions, and the anomalous behaviors of Ce and Eu often add difficulty to the recognition of tetrad effect.

In general, there is a tendency for ionization energy to rise with the increasing nuclear charge. But the case is a little complicated as far as the lanthanide series is concerned (Table 1.2). The third ionization energies (I_3), which account for the energies needed to remove the third electron from Ln^{2+} to form Ln^{3+}, increase steadily from La to Eu, then an abrupt drop shows up at Gd, and the increasing trend repeats until another drop comes out at Lu. By reviewing the electron configurations of lanthanide atoms, we can find that the low I_3 values for Gd and Lu are closely related to the electrons in 5d subshells, and that the high I_3 values for Eu and Yb show close correlations with the extra stable states of half and fully filled 4f subshells, respectively.

1.2.2 4f electrons of Ln^{3+}

There are seven electron orbitals permitted in the 4f subshell (Table 1.3), and the Pauli Exclusion Principle only allows two electrons with opposite spins in each orbit,

f orbital	La^{3+}	Ce^{3+}	Pr^{3+}	Nd^{3+}	Pm^{3+}	Sm^{3+}	Eu^{3+}	Gd^{3+}	Tb^{3+}	Dy^{3+}	Ho^{3+}	Er^{3+}	Tm^{3+}	Yb^{3+}	Lu^{3+}
m_l=+3		↑	↑	↑	↑	↑	↑	↑	↑↓	↑↓	↑↓	↑↓	↑↓	↑↓	↑↓
m_l=+2			↑	↑	↑	↑	↑	↑	↑	↑↓	↑↓	↑↓	↑↓	↑↓	↑↓
m_l=+1				↑	↑	↑	↑	↑	↑	↑	↑↓	↑↓	↑↓	↑↓	↑↓
m_l=0					↑	↑	↑	↑	↑	↑	↑	↑↓	↑↓	↑↓	↑↓
m_l=-1						↑	↑	↑	↑	↑	↑	↑	↑↓	↑↓	↑↓
m_l=-2							↑	↑	↑	↑	↑	↑	↑	↑↓	↑↓
m_l=-3								↑	↑	↑	↑	↑	↑	↑	↑↓
Σm_l (=L)	0	3	5	6	6	5	3	0	3	5	6	6	5	3	0
L	S	F	H	I	I	H	F	S	F	H	I	I	H	F	S
Σs_Z(=S)	0	1/2	1	3/2	2	5/2	3	7/2	3	5/2	2	3/2	1	1/2	0

Table 1.3 Electrons in 4f orbitals of Ln^{3+}.↑ is the up-spin electron with s=1/2,↓ is the down-spin electron with s=-1/2.

namely up-spin electron (s=1/2) and down-spin electron (s=-1/2). This is the reason

why 4f subshells can accommodate14 electrons at most. Electrons being added into these orbitals must abide by the Hund's rules. Therefore, from La^{3+} with a totally empty 4f subshell, electrons of same spin (s=1/2) are assigned into seven orbitals until the 4f subshell reaches its half-filled state at Gd^{3+}, which means each orbital is occupied by an un-paired electron. As seven orbitals in 4f sub-shell are seized by the up-spin electrons, no more up-spin electrons are allowed to enter into 4f subshell, and from Tb^{3+}, the down-spin electrons (s=-1/2) begin to occupy 4f orbitals until each 4f orbital holds a pair of electrons.

	electronic configuration	*S*	*L*	*J*	ground state term ($^{2S+1}L_J$)
La^{3+}	[Xe]	0	0	0	$^1S_0$
Ce^{3+}	$[Xe]4f^1$	1/2	3	5/2	$^2F_{5/2}$
Pr^{3+}	$[Xe]4f^2$	1	5	4	$^3H_4$
Nd^{3+}	$[Xe]4f^3$	3/2	6	9/2	$^4I_{9/2}$
Pm^{3+}	$[Xe]4f^4$	2	6	4	$^5I_8$
Sm^{3+}	$[Xe]4f^5$	5/2	5	5/2	$^6H_{5/2}$
Eu^{3+}	$[Xe]4f^6$	3	3	0	$^7F_0$
Gd^{3+}	$[Xe]4f^7$	7/2	0	7/2	$^8S_{7/2}$
Tb^{3+}	$[Xe]4f^8$	3	3	6	$^7F_6$
Dy^{3+}	$[Xe]4f^9$	5/2	5	15/2	$^6H_{15/2}$
Ho^{3+}	$[Xe]4f^{10}$	2	6	8	$^5I_8$
Er^{3+}	$[Xe]4f^{11}$	3/2	6	15/2	$^4I_{15/2}$
Tm^{3+}	$[Xe]4f^{12}$	1	5	6	$^3H_6$
Yb^{3+}	$[Xe]4f^{13}$	1/2	3	7/2	$^2F_{7/2}$
Lu^{3+}	$[Xe]4f^{14}$	0	0	0	$^1S_0$

Table 1.4 S is the total spin quantum number, L represents the total orbital angular momentum quantum number, and J denotes the total angular momentum quantum number

From La^{3+} to Gd^{3+}, due to the progressive accumulation of the electrons of parallel spin within the 4f subshell, the total spin quantum number *S*, which is the sum of spin quantum numbers of 4f electrons, gradually increases from f^0 (La^{3+}) to its maximum value of 7/2 at the half-filled point f^7 (Gd^{3+}). Afterward, the successive addition of the electron with reverse spin into the 4f subshell leads *S* to a decrease from 7/2 to 0 at Lu^{3+} with a fully filled 4f subshell (Table 1.4).

Since there are less than two electrons in 4f, La^{3+} and Ce^{3+} are not influenced by the

inter-electron repulsion of 4f electrons. For the rest Ln^{3+}, the inter-electron repulsion can be quantitatively described with a set of Racah parameters, which are generally obtained empirically from spectroscopic studies. There are four Racah parameters, E^0, E^1, E^2 and E^3, but E^2 is not involved for energy expressions for ground terms. E^0, E^1 and E^3 are related with the inter-electron repulsion. As the 4f subshell contracts, which is a result of the increasing protons in the nucleus, the inter-electron repulsion between 4f electrons arises, and E^1 and E^3 show steady increases. The reported values of Racah parameters for free gaseous Ln^{3+} and aqua Ln^{3+} are exhibited in Table 1.5. When E^1 and E^3 are plotted against the atomic number, they roughly show linear correlations (Fig. 1.2).

	(cm^{-1})	Pr	Nd	Pm	Sm	Eu	Gd	Tb	Dy	Ho	Er	Tm
free Ln^{3+}	E^0	210000	219000	226000	234000	241000	248000	254000	260000	266000	272000	278000
	E^1	6640	6930	7180	7400	7630	7870	8030	8200	8390	8570	8750
	E^2	36.7	38.3	39.6	40.9	42.2	43.5	44.4	45.4	46.4	47.4	48.4
	E^3	704	734	761	785	809	834	851	869	890	910	929
aqua Ln^{3+}	E^1	4550	4740	4920	5500	5570	5760	6020	6120	6440	6770	7140
	E^3	467	486	526	556	557	582	609	610	624	647	674

Table 1.5 The values of Racah parameters for free and aqua Ln^{3+} (cm^{-1}). Racah parameters for free Ln^{3+} are cited from Fraga and Karwoski (1974), and Racah parameters for aqua Ln^{3+} are determined by Carnall et al. (1968a, b, c and d).

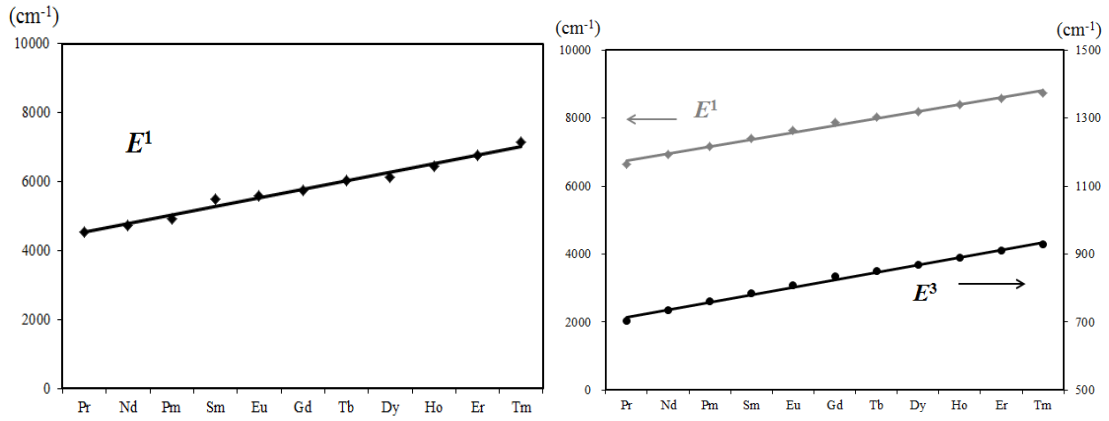

Figure 1.2 Racah parameters (E^1 and E^3) of Ln^{3+} are plotted against the atomic number of lanthanide. The left one is aqua Ln^{3+}, and the right one is free Ln^{3+}.

It has been well established that there will be a decrease in Racah parameters when

the free Ln^{3+} ions coordinate with ligands to form complexes and compounds, which in turn means a decrease in the inter-electron repulsion between 4f electrons. For instance, when the water molecules are attached to the free lanthanide ions, a slight decrease in Racah parameters is expected. This phenomenon is called nephelauxetic effect, which comes from the Greek for cloud-expanding, and now is a widely used term for the transition metals. In other words, the direct consequence of the transformation from free Ln^{3+} ions to the Ln^{3+} ions in certain coordination states is the decreases in Racah parameters (E^1 and E^3), which are used to describe the inter-electron repulsion energies (Reisfeld and Jorgensen, 1977; Jorgensen, 1979). From experimental observations, for a series of ligands with a common Ln^{3+}, the nephelauxetic effect grows in the following order (Tchougreeff and Dronskowski, 2009).

$$F^- < H_2O < NH_3 < NCS^- < Cl^- < CN^- < Br^-$$

1.2.3 The energy states of 4f electrons of Ln^{3+}

In 1962, Jørgensen, a famous scientist in spectroscopy, set up a theoretical equation to account for the lowest energies of transition for electron transfer ($4f^q \rightarrow 4f^{q+1}$), f-f excitation ($4f^q \rightarrow 4f^{q-1}$) and f-d excitation ($4f^q \rightarrow 4f^{q-1}5d$) of lanthanide, on the basis of Slater-Condon-Racah theory for the atomic spectroscopy. His equation has been proved reliable by a series of spectroscopic studies about the Ln^{3+} (Loh, 1966; Nugent et al., 1971; Nugent et al., 1973), and this equation was later called as refined spin pairing energy theory (Reisfeld and Jorgensen, 1977; Jørgensen, 1979), which is short for RSPET. According to this theory, the lowest energy state of the electron in 4f sub-shell of Ln^{3+} can be expressed as the following equation,

$$E(4f^q) = qW_0 + (1/2)q(q-1)[E^0 + (9/13)E^1] + (9/13)n(S)E^1 + m(L)E^3 + p(S,L,J)\zeta_{4f} \qquad (1.1)$$

In equation (1.1), q denotes the number of 4f electrons; W_0 corresponds to the one-electron energy for 4f electron with the xenon core as in Griffith (1964) and Goldschmidt (1978). E^0, E^1, and E^3 are Racah parameters. The sum of the first two terms on the right side stands for the stabilization of 4f electrons due to the systematical increase of the effective nuclear charge from one element to the next. ζ_{4f} signifies the spin-orbit coupling constant, and $n(S)$, $m(L)$, and $p(L,S,J)$ are the constant coefficients derived from the Russell-Saunders coupling. Their values are summarized in Table 1.4. In Fig.3, the variation of $(9/13)n(S)$ exhibits a breakpoint at Gd^{3+}, while

$m(L)$ yields two cusps at between Nd^{3+} and Pm^{3+}, and at between Ho^{3+} and Er^{3+}. *S, L*, and *J* are abbreviations representing total spin angular momentum, total orbital angular momentum and total angular momentum.

Ln^{3+}	*q* of 4f	$n(S)$	$m(L)$	$p(L,S,J)$
La	0	0	0	0
Ce	1	0	0	-2
Pr	2	-1	-9	-3
Nd	3	-3	-21	-7/2
Pm	4	-6	-21	-7/2
Sm	5	-10	-9	-3
Eu	6	-15	0	-2
Gd	7	-21	0	0
Tb	8	-15	0	-3/2
Dy	9	-10	-9	-5/2
Ho	10	-6	-21	-3
Er	11	-3	-21	-3
Tm	12	-1	-9	-5/2
Yb	13	0	0	-3/2
Lu	14	0	0	0

Table 1.5 Coefficients for the free lanthanide Ln^{3+} ions. $n(S)$, $m(L)$ and $p(L,S,J)$ are cited from Kawabe (1992); E^1 and E^3 for free Ln^{3+} are from Fraga and Karwoski (1974).

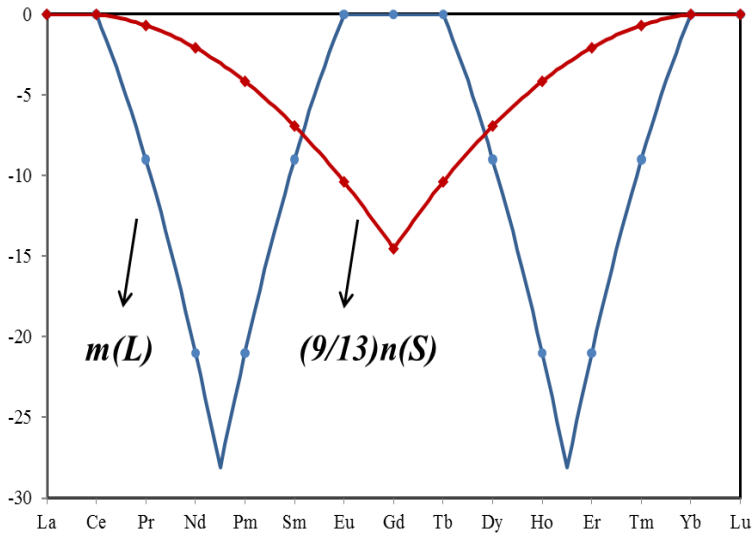

Figure 1.3 Variations of the coefficients of E^1 and E^3 Racah parameters.

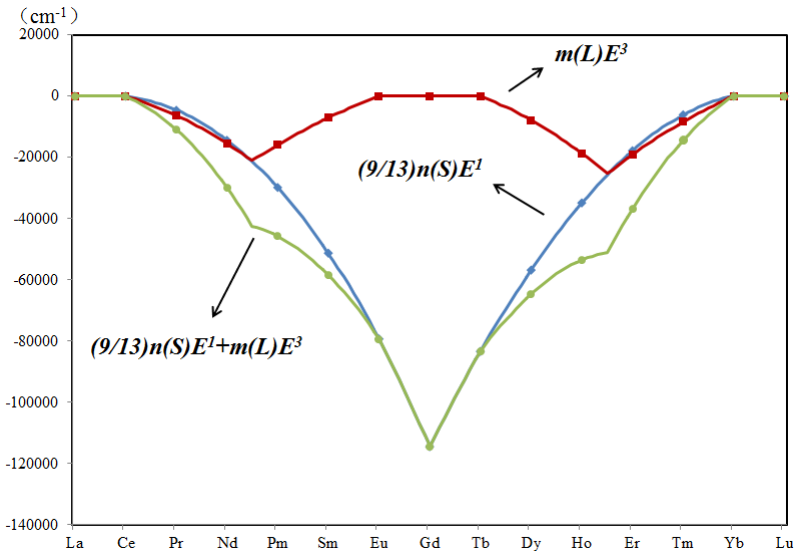

Figure 1.4 The inter-electron repulsion energy of free Ln^{3+}.

This equation reveals a fact that the energy state of a specific Ln^{3+} ion is mainly composed of three parts. The energy variation induced by the growing electrostatic interactions between nuclei and 4f electrons is described by a quadratic function of q, which is made up of the first two terms on the right hand side. Apparently, this function is only able to yield a smooth variation across the lanthanide series. The combined effort of the third and the forth term portrays the inter-electron repulsion between 4f electrons, whereas the last term denotes the spin-orbit interaction. In Fig. 1.4, the variation of $m(L)E^3$ of free Ln^{3+} displays two troughs at between $4f^3$ and $4f^4$, and at between $4f^{10}$ and $4f^{11}$, which can be associated with the first breakpoint and the third breakpoint in the tetrad effect, respectively. Meantime, the variation of $(9/13)n(S)E^1$ obviously corresponds with the half-filled effect (Fig. 1.4). The joint effort of them brings out the tetrad-effect-like variation for free Ln^{3+}. In comparison, the spin-orbit interaction, presented by $p(S,L,J)\zeta_{4f}$, generally makes minor contribution to the energy state of 4f electron. Hence, when the smooth energy variation is joined by the inter-electron repulsion, the overall variation of the lowest energy states of 4f electrons itself makes up four tetrads (Fig. 1.4).

1.2.4 The difference in ground state energy between two Ln^{3+} species

By now, we have focused our discussions on free gaseous Ln^{3+}, and figured out that the lowest energy states of 4f electrons in free Ln^{3+} ions produce an irregular variation, due to the inter-electron repulsion. Also, we have mentioned that, as Ln^{3+} ions bind with different ligands, the Racah parameters will change in response to the different

extent of nephelauxetic effect. For example, the lowest energy level of the 4f electronic configuration for the Nd^{3+} ion coordinated with O^{2-} is different from that coordinated with F^-. According to the refined spin pairing energy theory, the lowest energy state difference ΔE can be written as below.

$$\Delta E = q\Delta W_0 + (1/2)q(q-1)[\Delta E^0 + (9/13)\Delta E^1] + (9/13)n(S)\Delta E^1 + m(L)\Delta E^3 + p(S,L,J)\Delta\zeta_{4f} \qquad (1.2)$$

Since Racah parameters are linear functions of the number of 4f electrons, the variation of the lowest energy differences across the lanthanide series would also comprise four tetrads.

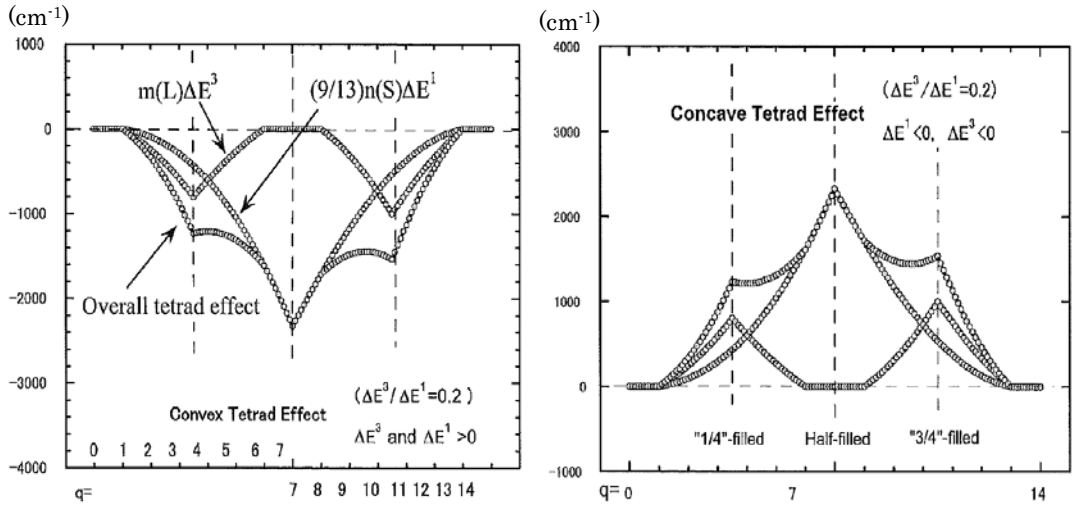

Figure 1.5 The variations induced by the differences in Racha parameters (Kawabe, 2008). The left graph is plotted when $\Delta E^1>0$, $\Delta E^3>0$; while the right one is plotted when$\Delta E^1<0$, $\Delta E^3<0$.

The systematic variations of $(9/13)n(S)\Delta E^1$, $m(L)\Delta E^3$ and $(9/13)n(S)\Delta E^1+m(L)\Delta E^3$, which are cited from Kawabe et al. (2008), are displayed in Fig. 1.5. The ratio of $(\Delta E^3/\Delta E^1)$ is presumed to be 0.2. If ΔE^1 and ΔE^3 both take positive values, the difference of inter-electron repulsions between two types of bondings will give rise to a tetrad effect in both cases. More precisely, when $\Delta E^1>0$ and $\Delta E^3>0$, it turns out to be a convex up tetrad pattern, while a concave down tetrad pattern shows up when both ΔE^1 and ΔE^3 take negative values.

In the thermodynamic reaction between two Ln^{3+} species, the knowledge of the difference in ground state energy of $[Xe](4f^q)$ electronic configuration is of great importance as this type of energy difference becomes an essential part of the enthalpy difference (ΔH) for the reaction, like Nugent (1970) has suggested in his theoretical interpretation for the tetrad effect found in the liquid-liquid extraction.

1.2.5 Improved RSPET for the tetrad effects in thermodynamics

The refined spin pairing energy theory tells us that slight differences in Racah parameters between two coordination states of Ln^{3+} can cause a tetrad effect to the systematic variation of the differences in the inter-electron repulsion energies between 4f electrons in the ground-levels of [Xe](4f^q) electronic configurations. However, the tetrad effect was first documented in the logK_d distribution pattern for the ligand-ligand extraction experiment of Ln^{3+}. How to link the tetrad effect illustrated by the spectroscopic theory with the tetrad effect observed in a thermodynamic reaction of Ln^{3+} is the primary concern in this chapter.

$$\text{Ln(III)-}X_{(aq)} + Y_{(org)} = \text{Ln(III)-}Y_{(org)} + X_{(aq)} \qquad (1.3)$$

In the above ligand-ligand exchange reaction (1.3), which is analogous to the reaction for the ligand-ligand extraction experiment by Peppard et al. (1969), *X* and *Y* represent two different kinds of ligands, and the lanthanide ions coordinate with different ligands before and after the reaction. As a result, the ground state energies of Ln^{3+} ions are expected to be different. Kawabe (1992) suggested that the difference in ground state energies (ΔE) would make an essential contribution to the enthalpy difference (ΔH_r) for this reaction. As a result, the tetrad effect of ΔE is absorbed into the variation of ΔH_r. But unfortunately, the parameters in this equation, like ΔW_0 and Racah parameters, are originally obtained from the spectroscopic observations, and they cannot be determined in the thermodynamic reaction. Hence, the equation derived from spectroscopic needs some modifications so as to become applicable to the thermodynamics.

As we have mentioned in the early context, there seems to be strong dependences of all Racah parameters on the number *q* of 4f electrons. In fact, it has already been pointed out that E^1 and E^3 are linear functions of *q* (Vander Slius and Nugent, 1972; Nugent et al., 1973). On the other hand, according to Condon and Odabasi (1980), W_0 is approximately proportional to the square of effective nuclear charge, which also can be expressed by *q* (Kawabe, 1992). The spin-orbit interaction constant ζ_{4f} is also expected to correlate with the forth power of effective nuclear charge. Therefore, all parameters on the right side of equation (1.2) can be expressed by the number *q* of 4f electrons in the following ways,

$$\Delta W_0 = f_w(q)Z^* = (C_w + C'_w q + \cdots)(q + s^*)^2$$

$$\Delta E_0 = f_a(q)Z^* = (C_a + C'_a q + \cdots)(q + s^*)$$

$$\Delta E^1 = f_1(q)Z^* = (C_1 + C'_1 q + \cdots)(q + s^*)$$
$$\Delta E^3 = f_3(q)Z^* = (C_3 + C'_3 q + \cdots)(q + s^*)$$
$$\Delta \zeta_{4f} = f_{ls}(q)Z^{*4} = (C_{ls} + C'_{ls} q + \cdots)(q + s^*)^4$$

$f_i(q)$ in these equations are polynomials of q, and s^* is the screen constant, taking the value of 25 (Kawabe, 1992). The sum of first two terms on the right side of equation (1.2) can be written as follows.

$$q\Delta W_0 + (1/2)q(q-1)[\Delta E^0 + (9/13)\Delta E^1] = q(q+25)\{(q+25)f_w(q) + (1/2)(q-1)[f_a(q) + (9/13)f_1(q)]\}$$
$$= q(q+25)(a + bq + cq^2 + \cdots).$$

Since W_0 is proportional only to the square of effective nuclear charge, it seems rational to neglect the quadratic and higher terms. Then, the equation (1.2) is eventually developed into the following form.

$$\Delta E = (a+bq)q(q+25) + (9/13)n(S)C_1(q+25) + m(L)C_3(q+25) + p(S,L,J)C_{ls}(q+25)^4 \qquad (1.4)$$

On the right side of equation (1.4), $p(S,L,J)C_{ls}(q+25)^4$ is used to describe the change in spin-orbit interaction energy between two different coordination states of Ln^{3+}. The difference in spin-orbit interaction energies between two coordination states becomes negligible. Therefore, this term will not be taken into consideration in this paper.

Since ΔE is an essential part of the enthalpy difference ΔH_r for the ligand-ligand exchange reaction (1.3), ΔH_r can be expressed by equation (1.5).

$$\Delta H_r = \Delta E + \Delta A \qquad (1.5)$$

A represents the energy difference that is not raised by the difference in ground state energy, and it is a constant. Combined with equation (1.4), ΔH_r is described as the following equation.

$$\Delta H_r = A + (a+bq)q(q+25) + (9/13)n(S)C_1(q+25) + m(L)C_3(q+25) \qquad (1.6)$$

On the right side of equation (1.6), A, a, b, C_1 and C_3 are constants, and their values can be determined by means of least-squares method, if ΔH is known in advance. Among them, C_1 and C_3 directly correlate with the differences in Racah parameters

ΔE^1 and ΔE^3, respectively. Through equation (1.6), ΔH_r for the thermodynamic reaction is also expected to display a tetrad effect. In the first application of this improved equation to the thermodynamic data of $LnO_{1.5}$ and LnF_3, Kawabe (1992) found that this equation could be applied to describe the tetrad effects both in lattice energies of LnF_3 and $LnO_{1.5}$ and in ΔH_r for the ligand exchange reaction between LnF_3 and $LnO_{1.5}$, and that the estimated values for ΔE^1 and ΔE^3 between NdF_3 and $NdO_{1.5}$ were in good agreement with the results obtained from spectroscopic studies.

1.2.6 Tetrad effects in ΔS_r and ΔG_r

For the ligand-ligand exchange reaction of Ln^{3+} conducted by Peppard et al., (1969), the systematic variation of the enthalpy differences ΔH_r is expected to display a tetrad effect, due to the changes in Racah parameters. As we have known, the $\log K_d$ pattern for the ligand-ligand exchange reaction also exhibits a tetrad effect. In this chapter, we are going to find out the relationship between the tetrad effect in ΔH_r and the tetrad effect in $\log K_d$.

Generally speaking, the difference in entropy ΔS_r for reaction (1.3) is composed of three parts, the difference in configuration entropy, the difference in electronic entropy, and the difference in vibrational entropy between two Ln^{3+} species (Denbigh, 1981). However, Kawabe (1999) argued that only the difference in vibration entropy $\Delta S_{r(Vib.)}$ makes a significant contribution to the ΔS_r for the ligand-ligand exchange reaction, because the difference in the configuration entropy between a pair of isomorphous Ln series is approximately constant across the series , and because the electronic entropies for Ln^{3+} ions are nearly the same between two Ln^{3+} species. In the same paper, Kawabe (1999) suggested that the systematic variation of $\Delta S_{r(Vib.)}$ is likely to show an analogous tetrad effect to ΔH_r, and so does the variation of ΔS_r across the lanthanide series, and that the tetrad effect in ΔS_r could also be expressed by the right side of equation (1.6). These suggestions were immediately confirmed by the thermodynamic data of $LnES_3 \cdot 9H_2O$ and $LnCl_3 \cdot 6H_2O$ (Kawabe, 1999).

In thermodynamics, the change in Gibbs free energy ΔG_r is equal to ($\Delta H_r - T\Delta S_r$). At a relatively low temperature, like the ligand-ligand extraction experiments performed by Peppard. (1969), the term of $T\Delta S_r$ becomes negligible, and the tetrad effect in ΔG_r is roughly the same with the tetrad effect in ΔH_r. For the ligand-ligand exchange experiments of Ln^{3+} carried out by Peppard et al. (1969), the minus contribution from $T\Delta S_r$ can be neglected, since the temperature is low, and there expected to be a tetrad effect in ΔG_r similar to that in ΔH_r.

In thermodynamics, the change in Gibbs free energy ΔG_r for reaction (1.3) can also be expressed by the equilibrium constant K.

$$\Delta G_r = -2.303RT \log K \qquad (1.7)$$

If the activity coefficient for each lanthanide ion does not vary remarkable from one to another, log$K$ on the right side of equation (1.7) corresponds to logK_d (Kawabe and Masuda, 2001). Then, ΔG_r is written as the follows.

$$\Delta G_r = -2.303RT \log K_d \qquad (1.8)$$

Through equation (1.8), the tetrad effect in logK_d pattern indicates that there a similar tetrad effect in $-\Delta G_r$, which is accordant with our expectation. For the ligand-ligand exchange experiments of Ln^{3+} carried out by Peppard et al. (1969), there is a tetrad effect in ΔH_r directly caused by the changes of Racah parameters for Ln^{3+} before and after the reaction. At a room temperature, the negative contribution from $T\Delta S_r$ is probably so small as not to significantly eliminate the tetrad effect in ΔH_r.

As suggested by Kawabe (1999) and Kawabe and Masuda (2001), the tetrad effects in ΔH_r, ΔS_r, ΔG_r and logK_d can be expressed by the right part of equation (1.6). However, these parameters (A, a, b, C_1 and C_3) for each tetrad effect have different meanings, and should be treated carefully.

1.2.7 The fitting of improved Jørgensen equation

In this section, we will use equation (1.9) to fit the tetrad effect in the logK_d pattern

$$\log K_d = A+(a+bq)q(q+25)+(9/13)n(S)C_1(q+25)+m(L)C_3(q+25) \qquad (1.9)$$

for the Ln^{3+} partitioning between H[DOP] (benzene) and HCl reported by Peppard et al. (1969).

Ln^{3+}	La	Ce	Pr	Nd	Pm	Sm	Eu	Gd	Tb	Dy	Ho	Er	Tm	Yb	Lu
logK_d	-2.99	-2.10	-1.69	-1.45	-0.89	-0.30	0.05	0.20	1.00	1.40	1.65	2.18	2.70	3.14	3.33
q of 4f	0	1	2	3	4	5	6	7	8	9	10	11	12	13	14

Table 1.6 The values of logK_d for Ln(III) between two solvent extracts [0.3M H[DOP] (benzene) and 0.05M HCl], and the number of 4f electrons of each lanthanide ions (Kawabe and Masuda, 2001).

When we put the logK_d value (Table 1.6) and the corresponding values of q, $n(S)$ and $m(L)$ for each lanthanide ion into equation (1.9), we can derive the following fourteen equations,

$-2.99=A+a\times0\times(0+25)+b\times0\times0\times(0+25)+(9/13)\times0\times C_1\times(0+25)+0\times C_3\times(0+25)$

$-2.10= A+a\times1\times(1+25)+b\times1\times1\times(1+25)+(9/13)\times0\times C_1\times(1+25)+0\times C_3\times(1+25)$

$-1.69=A+a\times2\times(2+25)+b\times2\times2\times(2+25)+(9/13)\times(-1)\times C_1\times(2+25)+(-9)\times C_3\times(2+25)$

.

.

.

$3.14=A+a\times13\times(13+25)+b\times13\times13\times(13+25)+(9/13)\times0\times C_1\times(13+25)+0\times C_3\times(13+25)$

$3.33=A+a\times14\times(14+25)+b\times14\times14\times(14+25)+(9/13)\times0\times C_1\times(14+25)+0\times C_3\times(14+25)$

Then, these simultaneous equations can be expressed by three matrixes in equation (1.10),

$$\boldsymbol{Y}=\boldsymbol{A}\times\boldsymbol{X} \tag{1.10}$$

where $\boldsymbol{Y}$ is $\begin{pmatrix} -2.99 \\ -2.10 \\ -1.69 \\ \bullet \\ \bullet \\ \bullet \\ 3.14 \\ 3.33 \end{pmatrix}$, and $\boldsymbol{A}$ represents $\begin{pmatrix} A \\ a \\ b \\ C_1 \\ C_3 \end{pmatrix}$

and $\boldsymbol{X}$ denotes $\begin{pmatrix} 1 & 0 & 0 & 0 & 0 \\ 1 & 0 & 0 & 0 & 0 \\ 1 & 2 & 4 & -18.6923 & -243 \\ \bullet & \bullet & \bullet & \bullet & \bullet \\ \bullet & \bullet & \bullet & \bullet & \bullet \\ \bullet & \bullet & \bullet & \bullet & \bullet \\ 1 & 13 & 169 & 0 & 0 \\ 1 & 14 & 196 & 0 & 0 \end{pmatrix}$

The matrix $\boldsymbol{A}$ can be worked out by several simple steps of matrix operations, and ultimately, it is expressed as $\boldsymbol{A}=(\boldsymbol{X}\times\boldsymbol{X}^{\boldsymbol{T}})^{-1}\times\boldsymbol{X}^{\boldsymbol{T}}\times\boldsymbol{Y}$. $\boldsymbol{X}^{\boldsymbol{T}}$ means the transport matrix of $\boldsymbol{X}$, and $(\boldsymbol{X}\times\boldsymbol{X}^{\boldsymbol{T}})^{-1}$ signifies the inverse matrix of $(\boldsymbol{X}\times\boldsymbol{X}^{\boldsymbol{T}})$. As each parameter in matrix $\boldsymbol{A}$ acquires its value, we can put them back into the equation, and obtain the regressed values of $\log K_d$, which make up the theoretical tetrad effect regressed by the equation. Here, fourteen equations are employed to determine the values of five parameters, and the

degree of freedom is nine. Consequently, the errors for all parameters raised by the least-squares method can also be calculated, according to the law of error propagation.

The fitting result is exhibited in Fig. 1.6. The regressed tetrad effect is nearly identical to the logK_d pattern, and displays four convex curves. Since A, a, b, C_1 and C_3 are determined with least-squares method, the logK_d pattern can be approximately expressed by them.

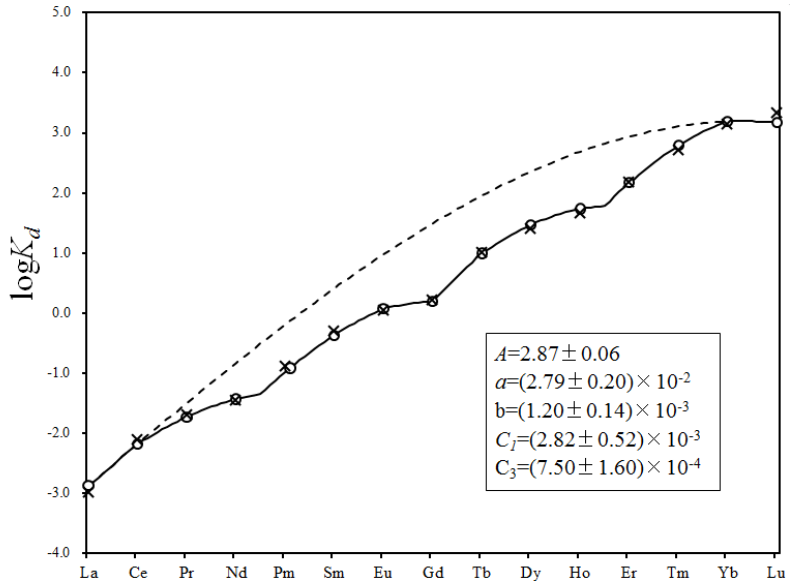

Figure 1.6 K_d is the partition coefficient of Ln^{3+} ion between 0.3M H[DOP](benzene) and 0.05M HCl. Crosses represent the regressed values for logK_d, and circles are the values reported by Peppard et al. (1969). The dashed line shows the smooth variation across the lanthanide series.

In fact, it is really difficult to figure out the significances of A, a and b. However, they are not the decisive parameters for the tetrad effect. In equation (1.9), C_1 and C_3 directly control the degree of tetrad effect. As we have discussed in the former section, the tetrad effect in logK_d corresponds with the tetrad effect in $-\Delta G_r$. Meanwhile, the tetrad effect in ΔH_r approximates to that in ΔG_r, because of the low temperature. Hence, the values of C_1 and C_3 for the tetrad effect in ΔH_r are supposed to be negative. Furthermore, since C_1 and C_3 for ΔH_r directly correlate with the differences in Racah parameters, ΔE^1 and ΔE^3 should also be negative, demonstrating a decrease in the inter-electron repulsion energy of 4f electrons.

In the earlier section, we have introduced the nephelauxetic effect for Ln^{3+}, showing that Racah parameters for 4f electrons of Ln^{3+} gradually decrease from F^- to O^{2-}. Based on the previous spectroscopic studies, Kawabe and Masuda (2001) argues

that the value of ($\Delta E^3/\Delta E^1$), or (C_3/C_1), for the nephelauxetic effect is likely to be a constant 0.23. For instance, the overall nephelauxetic effect for Nd^{3+} is estimated to be 0.23 (Fig. 1.7). However, there is another important fact that can be obtained from Fig. 1.7. If the Racah parameters for Ln^{3+} in two species are very close (e.g. $NdAlO_3$ and $Nd_2Te_4O_{11}$), it becomes quite possible that the ratio of ($\Delta E^3/\Delta E^1$) will deviate from 0.23.

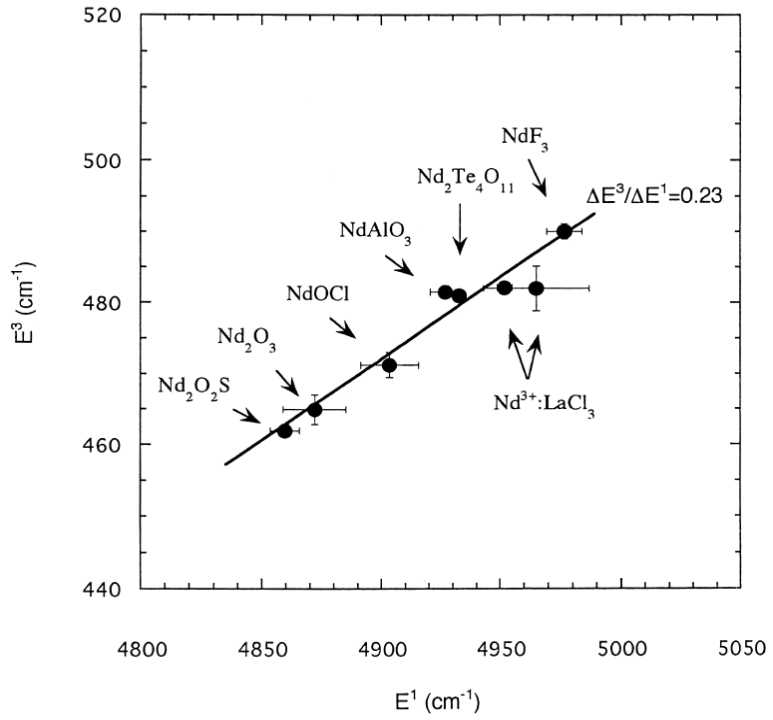

Figure 1.7 The nephelauxetic effect for Nd^{3+} defined by the Racah parameters in a couple of compounds. This graph is cited from Kawabe and Masuda (2001).

1.2.8 Disturbance to tetrad effect from the structural change

When Ln^{3+} ions coordinate with different ligands to form various compounds, the number of ligands potentially packed around Ln^{3+} is also variable, ranging from 2 to 12. Among them, the two most common coordination numbers are 8 and 9. Even when the lanthanide ions are coordinated with the same types of ligands, the number of ligands that each Ln^{3+} is able to accommodate would also show a decrease from light lanthanides to heavy lanthanides, due to the intrinsic lanthanide contraction. Then, a structural change shows up across the lanthanide series. The best known example is the hydrated Ln^{3+} (Habenschuss and Spedding, 1980; Rizkalla and Choppin, 1991). The light lanthanides ions (La^{3+}~Eu^{3+}) are able to accommodate nine water molecules, and the heavy lanthanides ions (Dy^{3+}~Lu^{3+}) are prone to coordinate

with eight water molecules, and the remaining lanthanides ions take both 8-fold and 9-fold coordination states. Although there are exceptions where the coordination number across the series keeps constant, they are really scarce. Therefore, when we study the tetrad effects between two Ln^{3+} species in the ligand-ligand exchange reactions, we need to be cautious whether there is a structural change having occurred across the entire lanthanide series, since the structural difference indeed brings an additional variation to the tetrad effect.

In a recent work, Kawabe (1999a) assessed the values of ΔH_r, ΔG_r and ΔS_r for the following ligand-ligand exchange reaction (1.11), basing on the previously published thermodynamic data for $LnCl_3 \cdot nH_2O$ and $LnES_3 \cdot 9H_2O$.

$$LnCl_3 \cdot nH_2O(c)+3(ES^-)(aq)+3H_2O(l)= LnES_3 \cdot 9H_2O(c)+3Cl^-(aq) \qquad (1.11)$$

On the left side of equation (1.11), the number of water molecules accommodated by Ln^{3+} in $LnCl_3 \cdot nH_2O$ changes from 7 for (La^{3+}~Pr^{3+}) to 6 for (Nd^{3+}~Lu^{3+}). In comparison, the production $LnES_3 \cdot 9H_2O$ is special, as the coordination number of each Ln^{3+} stays the same across the lanthanide series. Due to the unilateral structural change of Ln^{3+} in $LnCl_3 \cdot nH_2O$, the tetrad effects in ΔH_r, ΔG_r and ΔS_r became irregular, and could not be regressed by the improved Jørgensen equation, if the structural change was not corrected.

1.3 How to evaluate tetrad effect

It has already been 45 years since the first report of tetrad effect made by Peppard et al. (1969), and the theoretical interpretation on tetrad effect has been provided by the refined spin pairing energy theory, which suggests the tetrad effect is an intrinsic property of Ln^{3+} originated from the inter-electron repulsion between 4f electrons. However, the tetrad effect has not received enough attention, and it is still subject to questions (McLennan, 1994). In fact, we acknowledge that there are several factors hampering the recognition of tetrad effect.

Although tetrad effect rises from the inter-electron repulsion between 4f electrons of Ln^{3+}, the tetrad effect recognized in logarithmic REE pattern cannot be directly related with the inter-electron repulsion energy, but reflects the tetrad effect in ΔG_r. As a matter of fact, the difference in inter-electron repulsion energy makes a direct contribution to ΔH_r, leaving a tetrad effect to the variation of ΔH_r. Due to the

influence from $T\Delta S_r$, it is not immediately sure that the variation of ΔG_r displays a tetrad effect, and the recognition of tetrad effect in logarithmic REE pattern is mainly restricted to the low temperature system, where ΔG_r is approximately equal to ΔH_r.

Besides the tetrad effects recognized from the ligand-ligand exchange reactions, the chondrite-normalized REE patterns of many natural samples have been suggested to exhibit tetrad effects in the past several decades (Fig. 1.6). However, it has to say that the extensively used chondrite normalization itself often brings troubles to the recognition of tetrad effect, since the chondrite normalization represents the integrate fractionation of Ln^{3+} after several successive geologic processes. For these reasons, the significance of tetrad effect is presently underestimated, and we need to evaluate the tetrad effect properly.

In geochemistry, the lanthanides are generally classified as high field strength elements (HFSE), one group of the incompatible elements. At present, it is widely accepted that the behaviors of incompatible elements in geologic processes are controlled by two prime parameters, ionic charge and radius (Goldschmidt, 1937; Möller, 1988; Beattie, 1994; Wood and Blundy, 2003).

In natural environments, lanthanide ions commonly tend to be trivalent, with exceptions of Ce^{4+} and Eu^{2+}. Owing to the lanthanide contraction, the effective ionic

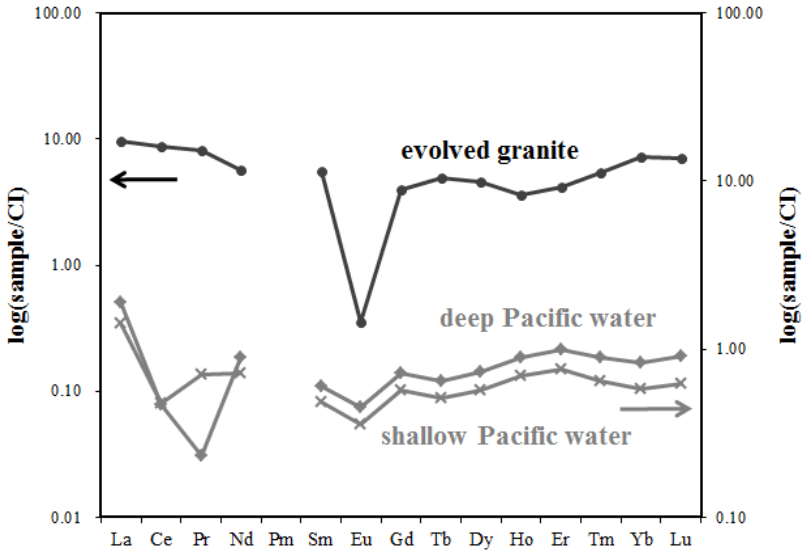

Figure 1.6 Tetrad effects reported from the chondrite-normalized REE patterns of natural samples. The evolved granite sample is from Irber (1999); and the Pacific water samples are from Piepgras and Jacobsen (1992).

radii of Ln^{3+} decreases systematically with the increase of atomic number (Shannon,

1976), but still, they have similar ionic radii, and show very similar electronegavities (Little and Jones, 1960). If the behaviors of lanthanides are wholly controlled by their incompatibilities in geological processes, the lanthanides are supposed to exhibit smooth variations without any remarkable irregularity in logarithmic patterns. Certainly, the smooth distribution patterns are quite common in most magmatic rocks or minerals (Albarède et al., 1997; Belousova et al., 2002; Chauvel and Hémond, 2000; Pearce et al., 1995).

However, we cannot ignore another fact that many more logarithmic patterns of lanthanides appear to show irregular variations. For example, the selective fractionation of either light or heavy lanthanides caused by certain minerals, like apatite and garnet, will result in an anomaly in the distribution pattern. On the other hand, there still remain some cases that can be covered neither by incompatibility nor by selective fractionation. The most typical example is the decoupling of Y-Ho. Yttrium and holmium are supposed to behavior coherently, but the nonchondritic ratios of Y/Ho have been reported in many studies (Kawabe et al., 1991; Bau, 1996; Irber, 1999; Jahn et al., 2001; Monecke et al., 2002). Apparently, Y-Ho decoupling contradicts the traditional interpretation on incompatible elements.

It is well known that aqueous fluids usually play important roles in various geologic events. These fluids are thought to carry abundant volatile components like H_2O and CO_2, and elements such as B, F, P and Cl (London, 1986; 1987). At the upper mantle, hydrothermal fluids, like carbonatite fluids, enriched in incompatible elements including lanthanides are considered as efficient metasomatism agents responsible for the enrichment character of basaltic rocks (Wass et al., 1980; Menzies and Murthy, 1980; Rudnick et al., 1993). In such fluids, those highly charged cations, like Y^{3+} and Ln^{3+}, may bind with ligands (e.g. F^-), and form various complexes (Ponader and Brown 1989; Keppler 1993). Bau (1996) argued that the complexation behavior of Ln^{3+}, which has a deep involvement with the electronic configuration of Ln^{3+}, is the primary reason for the decoupling of Y-Ho, and for the irregular distribution pattern of lanthanides. Therefore, for those where aqueous fluids are present, the behaviors of Ln^{3+} will no longer be solely controlled by their charges and radii, and the tetrad effect of Ln^{3+} should be taken into considerations.

According to the refined spin pairing energy theory, tetrad effect is an essential property of Ln^{3+}. Tetrad effect governs the behaviors of Ln^{3+} in the ligand-ligand exchange reactions. On the other hand, the imprint of tetrad effect has also been discerned in those geological processes involving an aqueous fluid activity. Thus, our

point is that the significance of tetrad effect should be reviewed, and the tetrad effect is an important factor to control the behavior of Ln^{3+}.

2. REE carbonate mineral assemblage in southwestern Japan

2.1 Kimuraite

Kimuraite is a hydrous REE carbonate mineral, and its chemical formula is written as $CaREE_2(CO_3)_4 \cdot 6H_2O$. In 1982, kimuraite was first found from the fissures of alkali olivine basalt located in Hizen-Cho, Higashi Matsuura-Gun, Saga Prefecture, Japan. Four years later, Nagashima et al. (1986) reported the chemical compositions and physical features of kimuraite. This mineral is actually named after the famous Japanese scholar, Professor Kenjiro Kimura, for his prominent contributions to the geochemistry and mineral chemistry of rare earth minerals.

According to Nagashima et al. (1986), kimuraite is a light purplish to pinkish white mineral, with a density of 2.60 g/cm^3, and there is a perfect cleavage along the {010} plane. The most impressive chemical feature of kimuraite is that it has a remarkably high abundance of REE, especially the Y-group rare earths, and the weight percent of rare earth oxides is up to 43%. However, the crystal structure of kimuraite has not been analyzed yet, and the coordination state of Ln^{3+} in kimuraite remains unknown. According to Miyawaki et al. (1993), kimuraite is structurally related to tengerite-(Y) [$Y_2(CO_3)_3 \cdot 2\text{-}3H_2O$], in which Y is 9-fold coordination. Thus, it seems that all REE^{3+} ions in kimuraite may occupy the same structural sites and take a same coordination number of 9.

Kimuraite is a very rare mineral, because it has been found from only two locations all over the world. One is in Japan, and the other one is the Pavlovskoe REE-coal Deposit, Khanka Lake, Primorskiy Kray, Far-Eastern Region, Russia. In this REE deposit, kimuraite was collected from the veins composed of water-bearing carbonate minerals. The REE compositions were reported by Seredin et al. (2009).

Akagi et al. (1993) conducted a study to investigate the REE compositions in three kimuraite samples collected from southwestern Japan, and came out with an interesting result that all the chondrite-normalized REE patterns of three samples exhibit similar concave tetrad effects (Fig. 2.1), with the negative Ce anomalies being ignored. Although Nagashima et al. (1986) measured the REE abundance of kimuraite, they did not normalize it to the chondritic abundance.

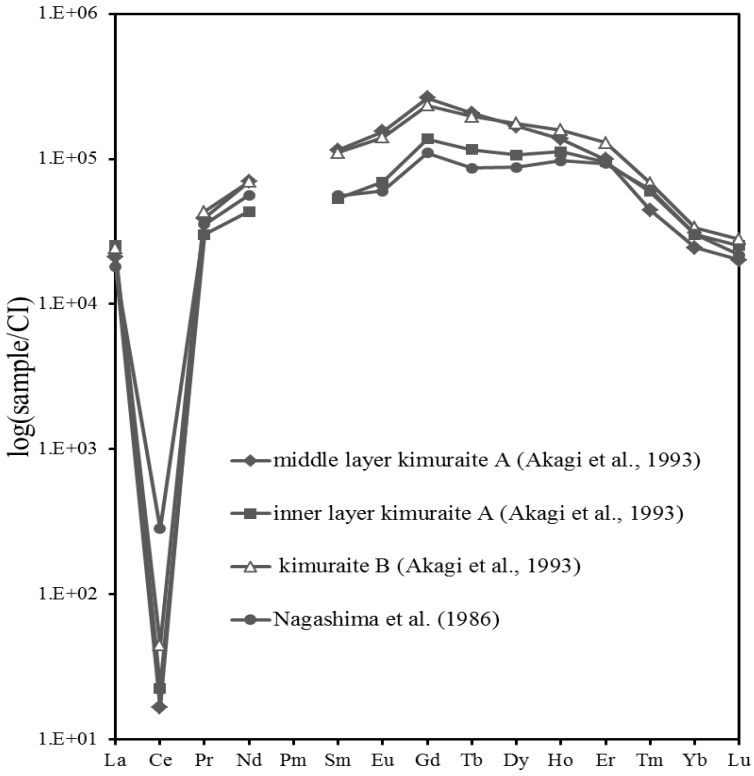

Figure 2.1 The chondrite-normalized REE patterns of kimuraite samples (Akagi et al., 1993)

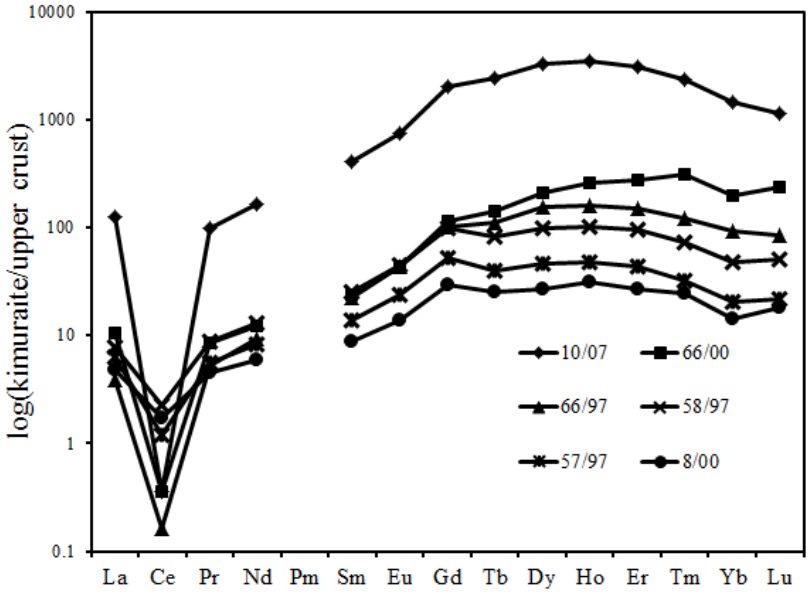

Figure 2.2 The upper crust normalized REE patterns of kimuraite samples (Serein et al., 2009). The upper crust values are from Taylor and McLennan (1985).

In contrast, the kimuraite samples analyzed by Seredin et al. (2009) were

normalized to the upper crust. In the upper crust normalized pattern (Fig. 2.2), a common point all these kimuraite samples share is the concave cusp at Gd, which is probably related to the octad effect (Kawabe et al., 2008).

2.2 Lanthanite

Lanthanite refers to another kind of REE carbonate minerals, and its chemical formula is written as $REE_2(CO_3)_3 \square 8H_2O$, from which we can see it is different from kimuraite. Ca is an essential element of kimuraite, but it is not admitted into the lattice

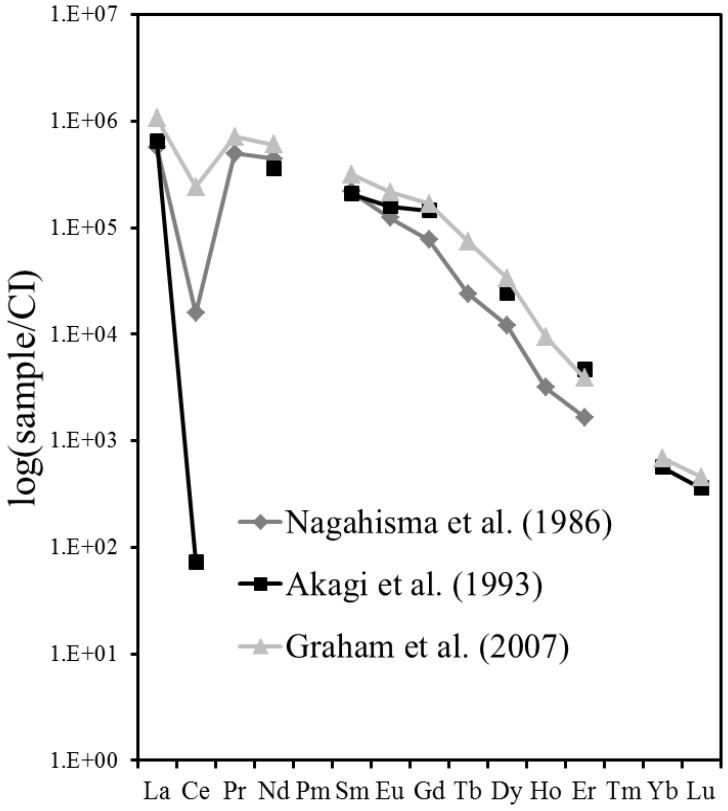

Figure 2.3 The chondrite-normalized REE patterns of three lanthanite samples.

of lanthanite. In contrast to the greater enrichment of Y-group rare earths in kimuraite, lanthanite is prone to preferentially incorporate light rare earths over Y-group rare earths (Fig. 2.3). As a result, lanthanite is nearly free of heavy rare earths, and only contains a small amount of yttrium. Three types of lanthanite have already been discovered at present, namely lanthanite-(La), lanthanite-(Ce) and lanthanite-(Nd). Lanthanite-(Nd) is a pink mineral under artificial light, while the other two types are

white. All three kinds of lanthanite show vitreous luster, and their crystals are flattened on {010} crystal plane and twinned on {010} plane. There is a good cleavage appearing along the {010} crystal plane. Its density is about 2.82 g/cm^3, a bit larger than that of kimuraite. According to Negro et al. (1977), the REE^{3+} ions in lanthanite seem to take the same coordination number of ten.

Up to now, lanthanite has been reported in many places across the whole world (Atencio et al., 1989; Bevins et al., 1985; Cesbron et al., 1979; Coimbra et al., 1989; Graham et al., 2007), whereas the occurrence of kimuraite has been restricted to two locations. Although kimuraite is considered as a coexisting mineral of lanthanite, it does not necessarily mean kimuraite and lanthanite always show up together. Either because of the trace amount of heavy REE in lanthanite, or because of the analytical problem, none of the previous studies on lanthanite has succeeded in determining the entire REE. The isotopic dilution method deployed by Akagi et al. (1996) was not capable of detecting the monoisotopic rare earths, including Pr, Tb, Ho and Tm, although Akagi et al. (1996) suggested the REE in lanthanite is likely to exhibit a tetrad effect when they normalized the REE abundances of their lanthanite sample to the REE abundances provided by Masuda et al. (1973) and Masuda (1975). In another paper, Graham et al. (2007) successfully analyzed the REE compositions of the lanthanite sample collected from Whitianga Hill with ICP-MS, except for Tm. Again from their chondrite-normalized REE pattern of lanthanite, a cusp showed up at Gd, which is thought to be a connection to the octad effect (Fig. 2.3).

2.3 Other carbonate minerals associated with kimuraite

Apart from kimuraite and lanthanite, there are other three types of REE carbonate minerals, including two new minerals, having been found from the same outcrop of alkali basalt in Japan. One of them is lokkaite.

Lokkaite was originally found by Vorma et al. (1966) from the pegmatite exposed at Kangasala in southwestern Finland, but it had been mistaken for tergerite until the main composition was analyzed by Perttunen (1971). In the later study, Nagashima et al. (1986) suggested the composition of lokkaite was not correctly determined due to contamination, and carefully examined the composition of the lokkaite collected from southwestern Japan with ICP-AES. According to this study, the chemical formula of lokkaite is defined as $CaY_4(CO_3)_7 9H_2O$. Like kimuraite, calcium and yttrium are the two prime elements. Lokkaite also has a remarkably high REE abundance, especially

the middle rare earth elements, and it displays a similar chondrite-normalized REE pattern to kimuraite (Fig. 2.4). Lokkaite is a snow white mineral, with a density of 2.92 g/cm^3.

Very recently, a new REE carbonate mineral, kozoite-(Nd), was reported by Miyawaki et al. (2000), and this mineral is named after Kozo Nagashima, in recognition of his outstanding effort to the mineralogy and crystallography of rare earth minerals. The chemical composition was measured with electron microprobe

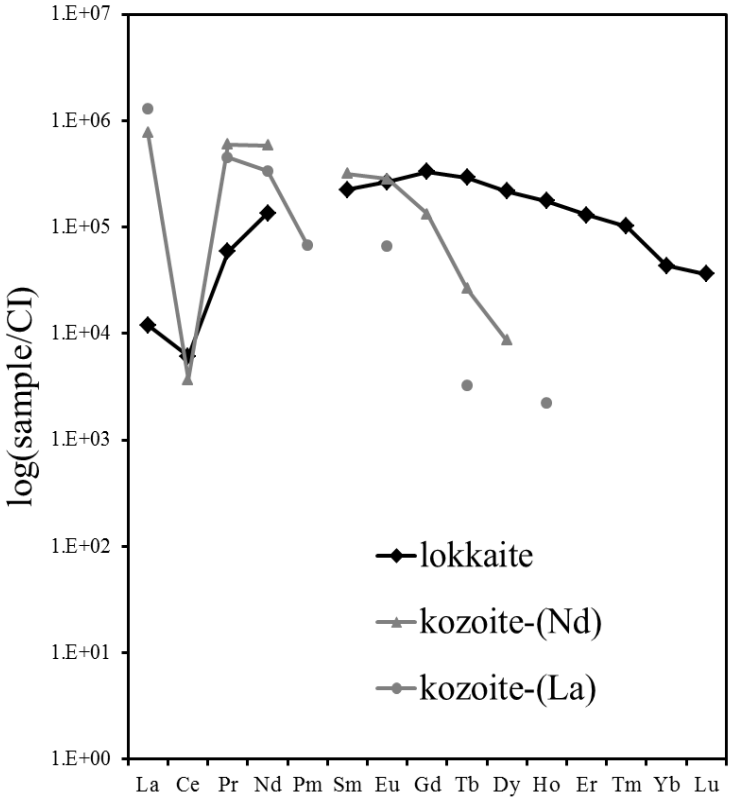

Figure 2.4 The chondrite-normalized REE patterns of lanthanite and kozoite from southwest Japan.

analyzer and CNH-elementary analysis, and the chemical formula was defined as (Nd,La,Ca)(CO_3)[(OH),(H_2O)]. Since calcium and absorbed water do not play crucial roles in kozoite, its formula is simply written as Nd(CO_3)(OH). Kozoite-(Nd) is pale pinkish purple to white in color with a vitreous to dull luster, and the density is calculated to be 4.77 g/cm^3. Soon after, another new mineral was described by Miyawaki et al. (2003). Its name is kozoite-(La), and the chemical formula is La(CO_3)(OH). Compared with kozoite-(Nd), lanthanum becomes the dominant rare earth in kozoite-(La), and besides this, only slight changes can be seen in their compositions. However, kozoite-(La) differs from kozoite-(Nd) in both chemical and

physical properties. For further information see Miyawaki et al. (2003).

2.4 Genesis of these carbonate minerals in Japan

From the alkali basalt in Japan, a couple of REE carbonate minerals have been identified, and these minerals can be classified into two types: one is the minerals comparatively enriched in Y-group rare earths, including kimuraite and lokkaite; another one is the minerals concentrating light rare earths, and lanthanite and kozoite belong to this group. Comparing all the carbonate minerals mentioned above, we can list two common features about them. First, the most amazing characteristic of these minerals is the extremely high abundance of REE, which definitely requires a REE mineralization in their source. And the second one is the absorbed water in each mineral. However, in order to disclose the genesis of the carbonate mineral assemblage, we need more hint.

Nagashima et al. (1986) proposed a simple hydration reaction of lokkaite to account for the genesis of kimuraite and lanthanite. But, Akagi et al. (1996) was apparently suspicious about this hydration reaction, because the mass balance of the reaction was not met. Lanthanite is often found alone, without the presence of either kimuraite or lokkaite (Coimbra et al., 1989; Graham et al., 2007), and this seems impossible if the hydration reaction works. Hence, Akagi et al. (1996) set up a new model to unravel the origin of kimuraite, in which kimuraite was suggested to be precipitated from an ore fluid carrying a large amount of rare earths. In Russia, a rare earth deposit, mainly composed of secondary REE carbonate minerals, was discovered in the walls and at the bottom of the Pavlovskoe REE ore body, which was intruded by basaltic dykes and sills. Seredin et al. (2009) attributed the formation of these carbonate minerals to a gas saturated and REE mineralizing fluid activity in the late stage of a basaltic magmatism. Since the carbonate mineral assemblage in southwest Japan is also tightly attached to the alkali basalt, it can be inferred the precipitation of these minerals probably resulted from a CO_2-rich hydrothermal fluid activity triggered by a basaltic magmatism event.

At present, there is no specific information we can rely on to constrain the formation temperature of the mineral assemblage in Japan, but there are some valuable clues offered by the relative studies. The occurrence of lanthanite in association with clinoptilolite in the Whitianga quarry implies that a low-T aqueous agent bearing a large amount of REE should be responsible for the subsequent precipitation of carbonate minerals (Graham et al., 2007). In the Pavlovskoe REE-coal

Deposit, along with the REE carbonate deposit, calcite veins were also observed, and the formation temperature of these veins was estimated to be around 150℃ (Seredin et al., 2009). Likewise, the lanthanite aggregations found at Santa Isabel by Coimbra et al. (1989) were accompanied by thin layers of calcite, and in southwestern Japan, the precipitation of calcite in the fissures of alkali basalt was also confirmed. Hence, it can be speculated, to a certain extent, that these secondary carbonate minerals in southwestern Japan might form at a temperature close to 150℃.

3. The occurrence of lanthanite in the cleavages of kimuraite

3.1 Background

Kimuraite, $CaREE_2(CO_3)_4 \cdot 6H_2O$, was first collected from an outcrop of alkali basalt in southwestern Japan, and its chemical and physical properties were studied by Nagashima et al. (1986). In the subsequent study, Akagi et al. (1993) reexamined the rare earths compositions of three kimuraite samples with ICP-MS, since the data obtained with ICP-AES in the pioneer work, from their point of view, did not seem convincible enough. In the chondrite-normalized REE pattern, all kimuraite samples displayed REE patterns that resemble the tetrad effect. Hence, they suggested that the chondrite-normalized REE pattern of kimuraite should be a tetrad effect. In their further discussions about the origin of tetrad effect, an ore fluid, which had formerly gained a tetrad effect through the water/rock interaction, was put forward by Akagi et al. (1996), and the tetrad effect in kimuraite was simply thought to be a duplication of the tetrad effect in precursor ore fluid.

Since all three samples studied by Akagi et al. (1993) were kimuraite, it is reasonable and necessary for them to show accordant compositions. However, the REE composition of one kimuraite sample, referred to as inner layer kimuraite of specimen A, is conspicuously different from other two samples, middle layer kimuraite of specimen A and kimuraite specimen B, as the former carries a relatively smaller amount of light REE while an equivalent amount of heavy REE to the latters. With regard to such a disagreement in compositions, Akagi et al. (1993) failed to shed light on it.

As far as the origin of tetrad effect in kimuraite is concerned, the discussions initiated by Akagi et al. (1996) are based on an assumption that the water/rock interaction is the only cause for the concave down tetrad effect, which is ultimately passed down to kimuraite. From the introduction of tetrad effect in the first chapter, we have learned that tetrad effect has the potential to emerge when the ligand exchange of REE^{3+} takes place. This is to say, it is not necessary for the precursor fluid to carry a tetrad effect as Akagi et al. (1996) suggested, since the ligand exchange during the transfer of REE^{3+} from the fluid to kimuraite is likely to produce

a tetrad effect.

Another spot where kimuraite has been found is the Abramovskoye ore in Russia, and Seredin et al. (2009) provided the REE compositions of six kimuraite samples, which were obtained with ICP-MS and X-ray phase analysis, but they did not offer any constructive comment on kimuraite. Comparing the REE compositions of kimuraite samples, we can note the REE abundances reported by Seredin et al. (2009) are one or two orders of magnitude smaller than those reported by Akagi et al. (1993). Moreover, in the upper-crust normalized REE patterns plotted by Seredin et al. (2009), the suggested tetrad effect of kimuraite in the chondrite-normalized pattern can not be discerned readily, instead, the Gd cusp, seen as a sign of the octad effect, can be recognized from each of the six samples.

In this work, we would like to continue the study on kimuraite, as we are curious about the REE pattern of kimuraite, and at the same time, we believe any effort on kimuraite is helpful for the better understanding of this rare species. We analyzed the composition of one kimuraite sample collected from Higashi-Matsuura District with ICP-AES, ICP-MS and electron probe micro-analyzer (EPMA), and finally, an unexpected but important fact was revealed by us.

3.2 Geologic settings

Cenozoic alkali basalts are sporadically distributed in the northeast China and around the Sea of Japan, and they are chemically different from ocean island basalt, and more like intraplate basalt (Uto et al., 1994; Uto and Tatsumi, 1996; Yanagi and Maeda, 1998). Nagamura et al. (1990) proposed the mixing of a depleted mantle source like MORB and an enriched source were necessary to account for the Sr-Nd-Pb isotope characters of these alkali basalts. However, the enriched source seems controversial. Nagamura et al. (1990) suggested it to be the mantle plume, but total volume of Cenozoic alkali basalt is small, and the spatial distribution also seems unlikely to be a result from the hotspot associated with mantle plume. There are more and more pieces of evidence showing that the metasomatism of upper mantle or lithospheric mantle, especially carbonate metasomatism, is of vital importance for the generation of alkaline magmas (Menzies and Murthy, 1980; Wass and Rogers, 1980; Dautria et al., 1992; Dupuy et al., 1992). Zhang et al. (2002) suggested that the enriched source for Cenozoic alkali basalt should be EM1, which could be produced by the metasomatised continental mantle lithosphere. Since the outcrop of Cenozoic

alkali basalt in southwestern Japan is not far away from the subduction zone, the enriched source might related to the metasomatism of continental mantle lithosphere by fluids from the dehydration of the subducted oceanic plate (Hawkesworth et al., 1990; Tatsumoto et al., 1992; Prouteau et al., 2001). This proposal is consistent with the weak modification of elements, like Nb, Ba and Ta, by subduction process (Nagamura et al., 1985; Nagamaru et al., 1989).

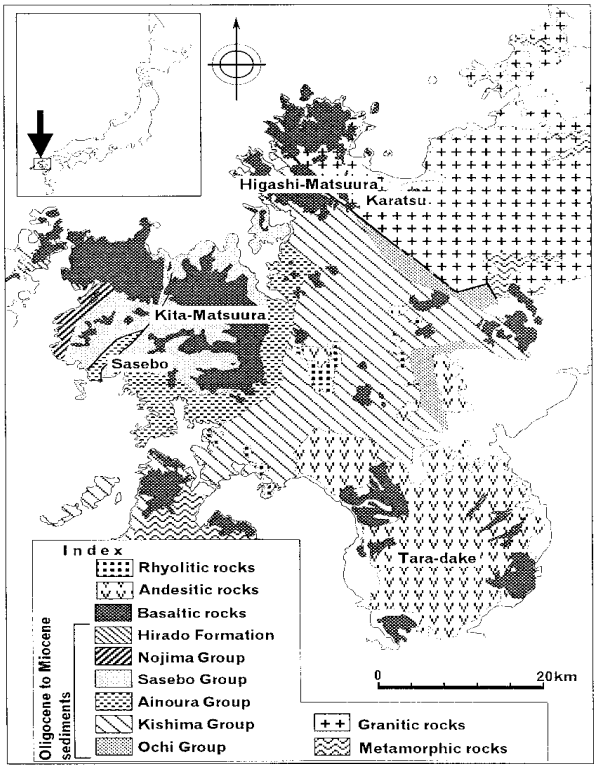

Figure 3.1 Geological map of northwestern Kyushu cited from Yanagi and Maeda (1998).

Fig. 3.1 is the geologic map of the southwest Japan, and the alkaline basalt exposed here also belongs to the Cenozoic basalt suite, and has been suggested to be the first-stage trachybasalt (Aoki, 1959). Our kimuraite sample was collected from the alkali olivine basalt exposed in Hizen Cho, Higashi Matsuura District, Saga Prefecture. The host basalt overlies the Pleistocene sedimentary rocks and the pre-Tertiary granodiorite, making up an unconformable contact. The alkali basalt appears to be a lava flow with a nearly horizontal flowage structure, and in its gray homogeneous groundmass, olivine phenocrysts, with a width reaching 2 mm, can be recognized. Kimuraite and other carbonate minerals are precipitated in the fissures of alkali basalt. The fissures are of various sizes, which can be up to l0 cm in length and 5 mm in width, and nearly run parallel to the flowage of alkali basalt.

Kimuraite occurs as spherulitic aggregates with a size of 4 cm long and 2 cm wide, and it is closely associated with coarser grained lanthanite, for instance, the specimen A studied by Akagi et al. (1993) showed a triple-layered structure, the outer layer was identified to be lanthanite by X-ray diffraction, while the middle and the inner layer were kimuraite. In some cases, kimuraite and lanthanite are found to be underlain by lokkaite, which forms snow-white spherulitic aggregates on fissure walls. In addition, instead of REE carbonate minerals, some fissures are filled with calcite and/or aragonite. For all fissures developed on alkali basalts, there is no implication for any later alteration.

3.3 Analytical methods

For our study, we only get one kimuraite sample, and for the sake of making full use of it, we first took one part from the sample, then, separated it into seven pieces, labeled as K-1, K-2, K-3, K-4, K-5, K-6 and K-7, and each piece weighed about 10 mg. The remaining part of kimuraite sample was put away.

First of all, we planned to determine the content of the absorbed water, one essential composition of kimuraite, in our kimuraite sample. According to Nagashima et al. (1986), kimuraite seems to lose its absorbed water thoroughly at a temperature around 55℃. We heated up the sample for two hours with an oven, of course the temperature is kept at 55℃, and by weighing the dried sample, we were supposed to know the amount of water. However, it proved to be more complicated than we had anticipated. The dried sample will start to absorb water from the air as soon as we take it out of the oven. We tried several times, but just could not measure the absorbed water precisely. Eventually, we gave up the determination of water.

In the second stage, all samples were heated at 800℃ for two hours. During this operation, the kimuraite samples will be completely decomposed, with carbon oxide released and calcium and REE oxides left. Then, the residual powder was dissolved with HCl. After this, the solution samples were prepared for the ICP determination.

Ca and REE compositions were first analyzed with ICP-AES. The spectral intervene was removed from the obtained data. Since the concentrations of REE were too high for the ICP-MS analysis, we, based on the result obtained with ICP-AES, diluted the solution samples, three hundred times dilution for the light rare earths whereas five hundred times dilution for the heavy rare earths. Ca and Y were not checked with ICP-MS, because they needed to be diluted for tens of thousands times.

Both ICP-AES and MS analyses were carried out at Department of Earth and Planetary Sciences, Nagoya University.

At the beginning, EPMA analysis was not in our plan, but when we figured out that the composition of our kimuraite sample determined with ICP-AES and MS was not accordant with those previously reported, the EPMA analysis becomes necessary.

Kimuraite in a conventional thin section was analyzed with JEOL JCXA-733 electron probe micro-analyzer at the Center for Chronological Research, Nagoya University. The analytical conditions are described as follows. The accelerating voltage was 15kV, the probe current was 25nA, and the probe diameter was 10μm with a counting time of 25s. Because kimuraite is abundant in volatile compositions, it makes hard to keep the analytical precision during the analysis. As a result, only five elements (Ca, Y, La, Pr and Nd) were able to be measured, and kimuraite was highly damaged by electron bombardment during the analysis. In this study, the method explored by Bence and Albee (1968) was adopted for matrix correction, using the α-factor table introduced by Kato (2005) with modification for Pr Lβ emission.

3.4 Results

The compositions of seven kimuraite sub-samples are summarized in Table 1. Ca and Y were determined with ICP-AES, while REE were determined with ICP-MS. The chondrite-normalized REE patterns are displayed in Fig. 3.1, and the chondrite values reported by Anders and Grevesse (1989) are used here. For comparison, the results obtained by Nagashima et al. (1986) and Akagi et al. (1993) were added into Table 1, and their chondrite-normalized patterns were plotted in Fig. 3.1 together. As we can see from Table 3.1, all kimuraite samples analyzed by us show exceedingly high abundances of REE. When compared with the others, our kimuraite samples show the highest abundances of lanthanum, varying from 6370 ppm to 20600 ppm. In contrast, two kimuraite samples, Specimen B and middle layer kimuraite A, apparently carry much more middle REE (Sm-Ho) than the other samples, especially Gd and Dy (Fig. 3.2). On the other hand, among all kimuraite samples, drastic differences are not found in heavy rare earths. For the three samples studied by Akagi et al. (1993), the contents of Y and Ca are not determined. Except for one sample (K-5), our kimuraite sub-samples have yttrium abundances close to Nagashima et al. (1986), but relatively smaller abundances of calcium. Because the absorbed water in our kimuraite samples is not determined, we are unable to calculate the chemical

formula for kimuraite. Instead, the mole ratios of ΣREE to Ca have been calculated, which range from 2.50 to 3.40. In fact, the recommended value of ΣREE to Ca for kimuraite is 2.00, it, thus, seems incredible that all the mole ratios for our kimuraite samples are much larger than that recommended one.

In the chondrite-normalized REE pattern, the extremely negative Ce anomaly is

	This study							Akagi et al. (1993)			Nagashima et al. (1986)
(ppm)	K-1	K-2	K-3	K-4	K-5	K-6	K-7	middle layer of kimuraite A	inner layer of kimuraite A	specimen B	
La	16900	12200	12600	7460	6370	13900	20600	4940	5970	5700	4270
Ce	7.15	6.47	7.04	10.8	4.62	9.43	8.45	10.0	13.6	27.0	170.0
Pr	4430	3920	4170	3380	2910	4720	5360	3490	2690	3860	3160
Nd	29100	28300	27500	24000	19100	31100	33200	31600	19600	31600	24900
Sm	10500	9330	8780	8660	8590	12100	12100	16900	7860	16300	8460
Eu	5130	5800	4140	4420	4160	5820	5730	8650	3880	7900	3370
Gd	28900	31000	25000	26900	20200	33500	32600	51700	27000	45900	21600
Tb	3860	4120	4100	4420	3120	4550	4470	7480	4210	7130	3160
Dy	22600	26500	23300	24800	21600	26400	25100	40700	25900	42800	21100
Ho	5170	5320	5750	6350	5230	5400	5360	7630	6220	8800	5430
Er	11800	12800	12900	14200	18300	12900	12600	15700	15100	20600	14800
Tm	824	936	1949	1732	1344	757	826	1080	1440	1650	1490
Yb	1924	2196	5359	4912	3349	1815	1981	3970	4880	5500	4910
Lu	219	250	653	605	403	206	224	489	614	683	532
Y	229000	265000	198000	211000	302000	231000	227000	-	-	-	231000
Ca	45100	50400	41900	45500	66200	43700	42300	-	-	-	65900
α	3.41	3.40	2.82	2.98	2.49	3.28	3.39	-	-	-	1.99

Table 3.1 The chemical compositions of kimuraite samples from southwest Japan. α is the mole ratio of ΣREE to Ca.

present in each sample. Cerium is very sensitive to the redox condition, and can be easily separated from the other REE. Akagi et al. (1993) attributed such an anomaly in kimuraite to the segregation of Ce^{4+} by water. When compared to the former studies, the abundances of LREE in our samples are much higher, while the HREE show a slight decrease (Fig. 3.2). The inner layer kimuraite A has a quite analogous REE to those of our subsamples (Fig. 3.1a and Fig. 3.2). Both the middle layer kimuraite A and kimuraite B reported by Akagi et al. (1993) show slight enrichments in middle

REE relative to other kimuraite samples. This agrees with the suggestion made by Kawabe et al. (2012) that the inner layer kimuraite A is enriched in La, Pr and Nd relative to the middle layer kimuraite A. In spite of these differences, all kimuraite samples exhibit similar concave tetrad effects.

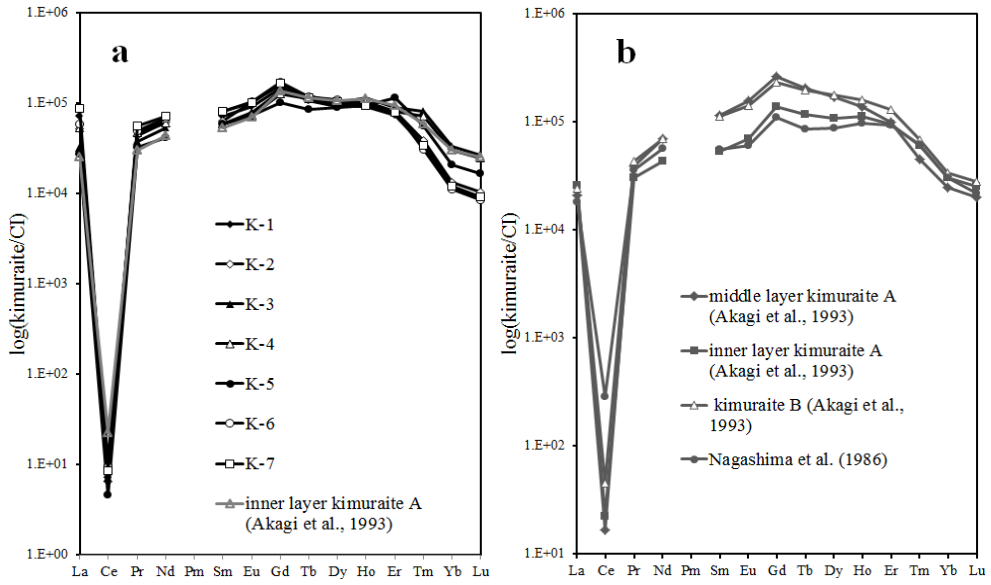

Figure 3.1 The chondrite-normalized REE patterns of our kimuraite samples are shown in graph a, while the chondrite-normalized REE patterns of other kimuraite samples are exhibited in graph b. Chondrite values are from Anders and Grevesse, (1989)

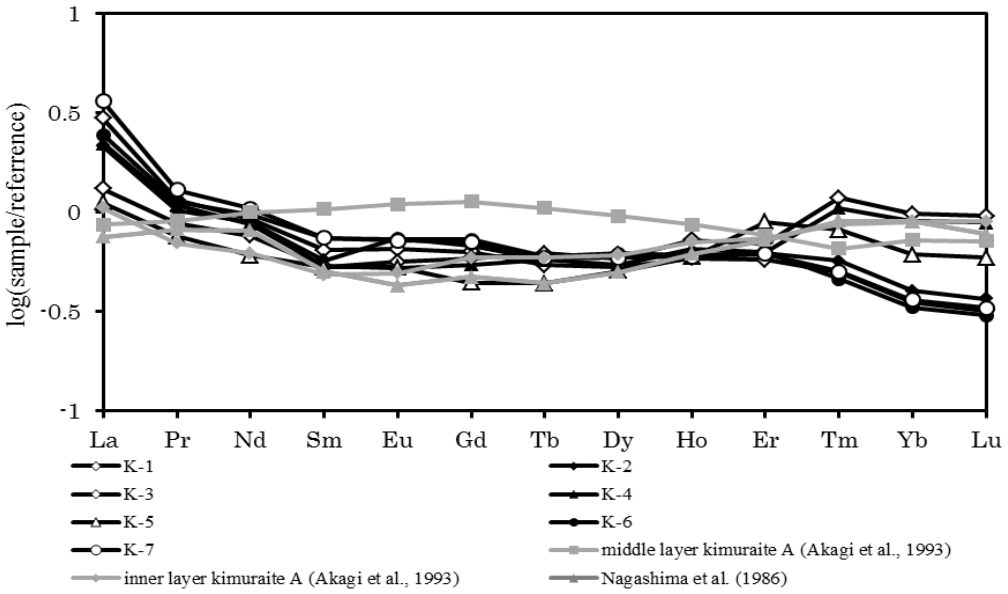

Figure 3.2 Kimuraite B analyzed by Akagi et al. (1993) is taken as a reference sample, and the REE abundances of other kimuraite samples are normalized to this reference sample in the logarithmic scale. Ce is not included in this plot, because of its negative anomaly.

Judging from the mole ratio of REE to Ca, our kimuraite sub-samples appear to have different compositions from that reported by Nagashima et al. (1986), though they show similar chondrite-normalized REE patterns. Therefore, we decided to examine the remaining part of our kimuraite sample with EPMA.

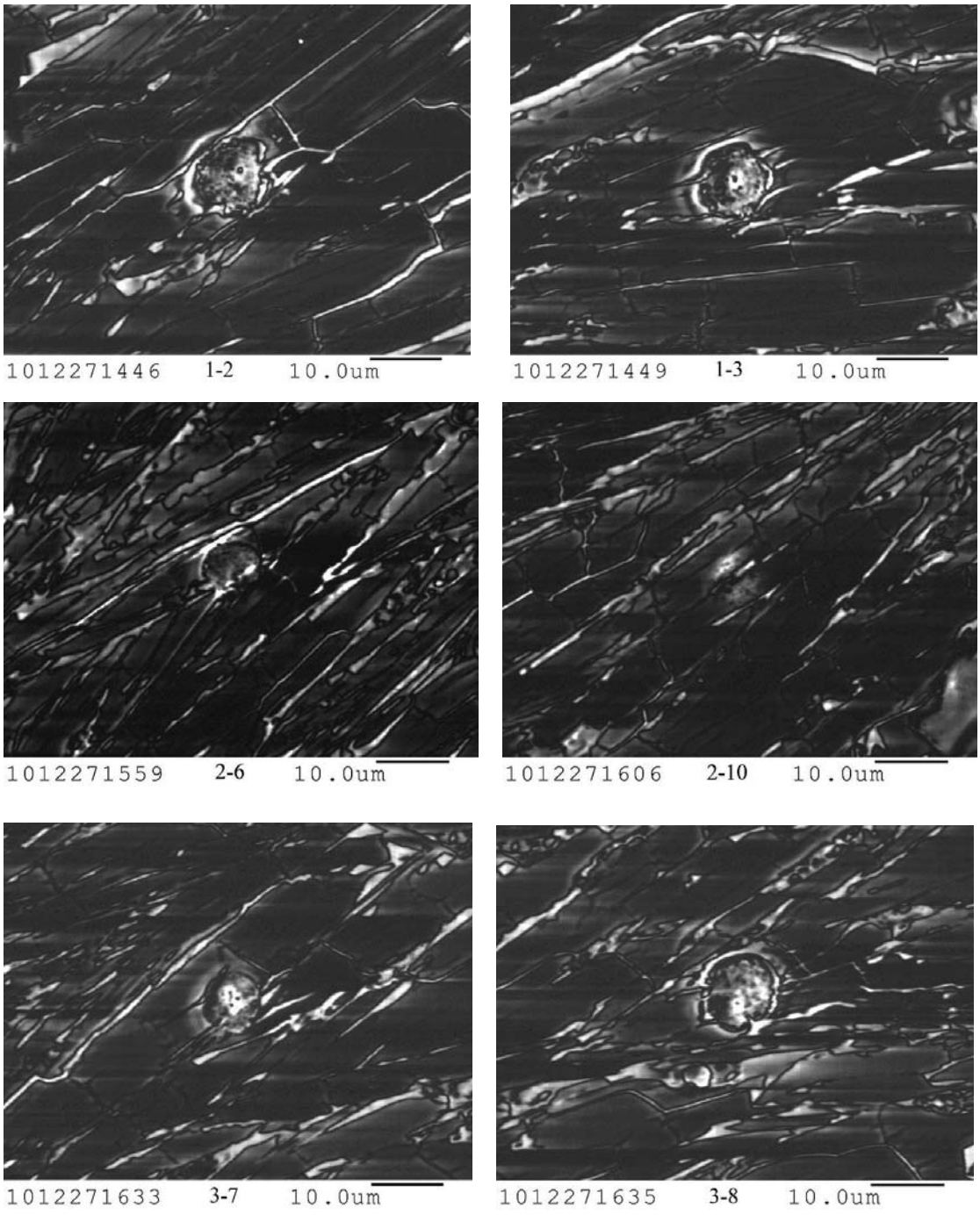

Figure 3.3 The backscattered electron images of our kimuraite samples. Dark parts are kimuraite, and the bright parts are another mineral that has different composition from kimuraite. Bright circles are the analysis spots by EMPA.

In Fig. 3.3 are the back-scattered electron (BSE) images of kimuraite. When the high energy electron beam, a part of electrons will be backscattered, and be captured by the detector, then, the back-scattered electron image will be produced. In general, the number of electrons backscattered from a sample is proportional to the mean atomic number of the target sample, on condition that the sample surface is smooth and flat. In other words, the brighter BSE intensity correlates with a greater average atomic number in the sample, and dark areas corresponds to a relatively lower average atomic number.

In these images of our kimuraite sample, two distinct parts can be seen, dark part and bright part, which correspond to a smaller and a larger mean atomic number, respectively. This, otherwise, means there is another mineral besides kimuraite. The dark part is kimuraite, since kimuraite is a mineral enriched in Ca and Y, both of which have relatively smaller atomic numbers. When kimuraite is to crystallize, a perfect cleavage will develop along the {0 1 0} crystal plane (Nagashima et al., 1986), and this cleavage can be well discerned in the BSE photos. Furthermore, it seems that the cleavage is filled with another mineral of bright BSE intensity. In light of the strong brightness in BSE photos, it can be inferred that the average atomic number of this mineral is much larger than kimuraite, namely, the composition is not the same with kimuraite. In fact, this is for the first time to recognize the existence of another mineral in kimuraite, and this must be the reason why there is a compositional disagreement between our kimuraite samples and the kimuraite from Nagashima et al. (1986).

Thirty-two spots were analyzed with EPMA, and the analytical results are listed in Fig. 3.4. The content of CaO ranges from 7.0% to 11.6%, and most of them are larger than the value of 9.2% determined by Nagashima et al. (1986). Y_2O_3 varies from 35.7% to 49.7%, all of which have exceeded the value of 29.4%. Here, it is noteworthy that the results obtained with EPMA clearly contradict with those obtained with ICP, since the ICP analysis came up with similar Y abundances and smaller Ca abundances when compared with Nagashima et al. (1986). It seems that the volatile components in kimuraite have brought a great disturbance into the EPMA analysis. The mole ratios of Σ(Y, La, Pr, Nd) to Ca are calculated to be 2.02 to 3.20, all of which are again greater than that proposed ratio. From the BSE photos, it can be noticed that nearly all the EPMA analysis spots failed to escape from the contamination of the bright part, in other words, all analyses have measured the compositions of mixtures which consist of kimuraite and a small portion of the

currently unknown mineral. Though the data obtained with EPMA might be doubtful, the BSE images have helped us reveal an important fact.

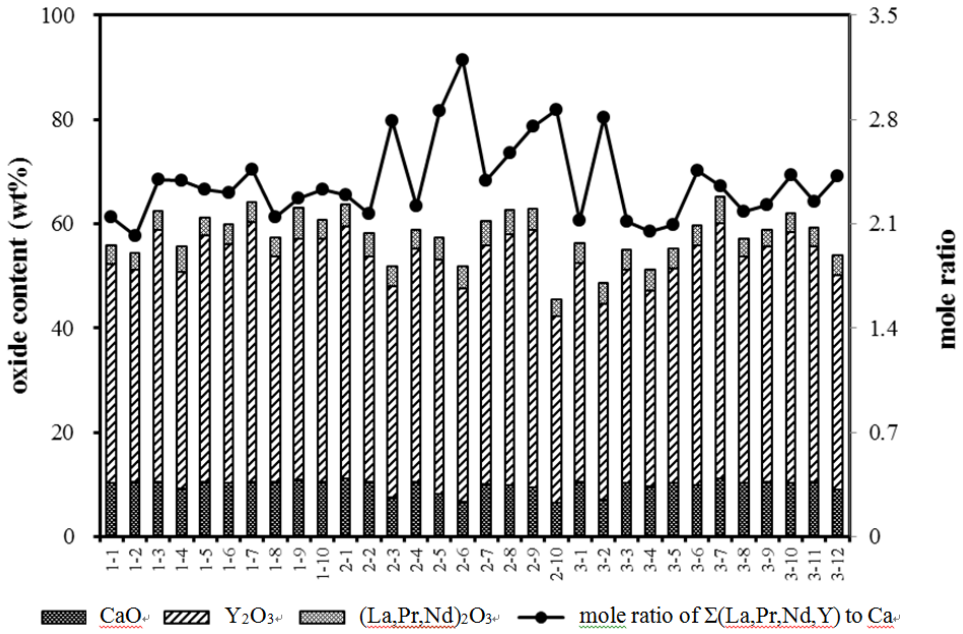

Figure 3.4 The compositions of thirty-two spots were analyzed with EPMA. Only five elements were able to be determined.

3.5 Discussions

In the pioneer work on kimuraite, Nagashima et al. (1986) defined the chemical formula of kimuraite as $CaREE_2(CO_3)_4 \bullet 6H_2O$, which was later approved by international mineralogical association (IMA). As for the seven kimuraite subsamples in our study, the mole ratios of REE against Ca determined with ICP-MS vary from 2.4 to 3.4, and all these values are much greater than the recommended value of 2.0. Given the analyzed minerals are the same in two studies, there should not be such a great disagreement on composition.

In the BSE photos, another mineral with brighter intensity precipitated in the cleavage of kimuraite is observed for the first time, demonstrating that our kimuraite samples are mixtures of two different minerals rather than a pure kimuraite. Due to the present of this mineral, which seems to have a relatively larger average atomic number than kimuraite, the compositions of our kimuraite sub-samples have suffered large alterations, which have been reflected from the mole ratios of REE to Ca. However, the mineral is too tiny for EPMA to directly locate the analysis spot on it to

specifically determine its composition. In our study, we chose to seek information from the available data, instead of doing other experiments to identify the composition of the mineral.

As already introduced in the former chapter, a couple of carbonate minerals have been reported from the same place in southwestern Japan, including kimuraite, lokkaite, lanthanite and kozoite, and all these minerals, without exception, are highly rich in REE. Among them, lokkaite and lanthanite are found having direct contact with kimuraite in both locations where kimuraite has been reported (Nagashima et al., 1986; Seredin et al., 2009). Hence, it seems reasonable to first take these two minerals into our consideration, when the bright mineral in our kimuraite sample is concerned.

Like kimuraite, lokkaite is also a carbonate mineral that enriches in Y-group rare earths, and contains a large amount of Ca (Table 2). But there is still a notable difference that lokkaite has much less lanthanum than kimuraite does. If a small amount of lokkaite is mixed with kimuraite, there supposed to be a remarkable reduction in the lanthanum abundance when this mixture is compared with the pure kimuraite. However, this is not in accordance with our result, as the average lanthanum abundance for our kimuraite samples is three times as high as the pure kimuraite analyzed by Nagashima et al. (1986). Furthermore, the great amount of Y and Ca in lokkaite will result in a weak BSE intensity like kimuraite, which is contradict to the strong brightness in our BSE images. Therefore, it can be inferred that the mineral present in our kimuraite is not lokkaite.

Lanthanite is another mineral closely associated with kimuraite. Akagi et al. (1993) reported that one of their kimuraite samples was covered by a layer of lanthanite. However, its chemical composition is quite different from kimuraite. Lanthanite is totally free of Ca and Y, which are two essential constituents in kimuraite. Compared to the tremendous amount of LREE, the HREE in lanthanite is relatively negligible (Nagashima et al., 1986; Coimbra et al., 1989; Graham et al., 2007). On one hand, the absence of lighter elements, like Ca and Y, will allow lanthanite to produce strong signals in the BSE imaging. On the other hand, if kimuraite is mingled with a small amount of lanthanite, the peculiar chemical composition of lanthanite will cause an increase to the LREE while a decrease to the HREE abundance of the mixture, which is coincident with the chondrite-normalized REE patterns of our kimuraite samples. Therefore, lanthanite is the most proper candidate for the contaminant mineral.

The chemical formula, $Ca(Y,REE)_2(CO_3)_4 \square 6H_2O$, tells us that the mole percentages of CaO and $(REE+Y)_2O_3$ in a pure kimuraite should be the same value 50%, if the

volatile parts are not taken into consideration. Since lanthanite does not contain any calcium, the REE_2O_3 mole percentage for a pure lanthanite will be 100%. In Fig. 3.5, the kimuraite sample analyzed by Nagashima et al. (1986) can be regarded as a pure kimuraite. Our kimuraite samples are distributed in the area close to the pure kimuraite, making up a linear trend toward the pure lanthanite. First of all, the possibility of kozoite being the contaminating mineral can be excluded. Although lokkaite is also plotted on this trend, it is impossible for lokkaite to be the contaminating mineral in our samples. One reason is that lokkaite is not capable of generating the strong BSE intensity as we have already seen in the images. In addition, if the contaminating mineral is lokkaite, the proportions of lokkaite need to be about 40%~80%, which is apparently not consistent with the observation of BSE images. Therefore, it can be concluded that our kimuraite sub-samples have been contaminated by lanthanite to different extents. Judging from this plot, the proportions of lanthanite in our kimuraite samples can also be estimated, ranging from 10% to 20%.

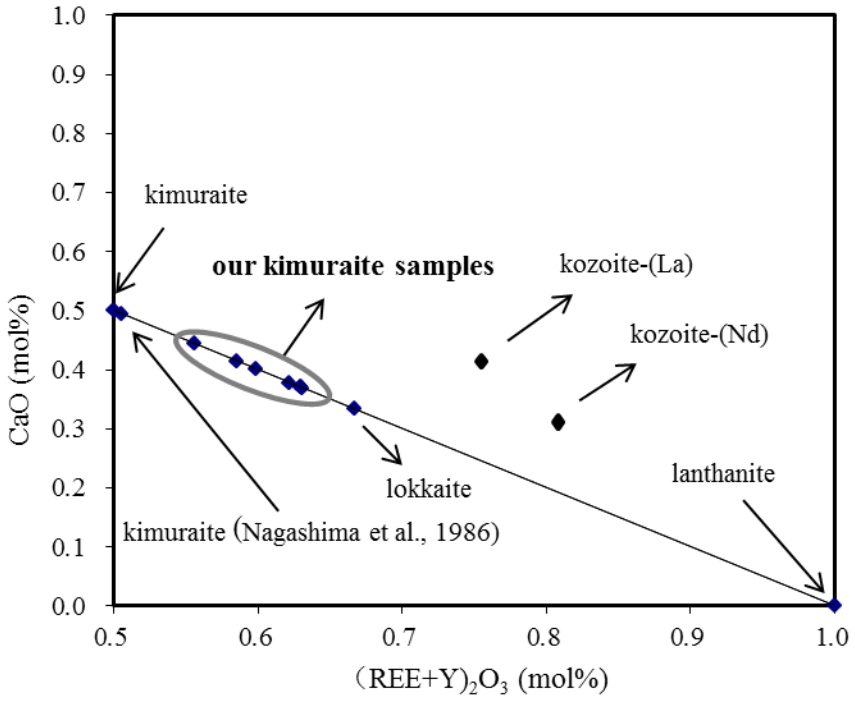

Figure 3.5 The mole fractions of $(REE+Y)_2O_3$ for carbonate REE minerals were plotted against their mole fractions of CaO. These values for the ideal kimuraite and the ideal lanthanite were calculated from their chemical formula, respectively.

Undoubtedly, the mineral filling in the cleavage of kimuraite is lanthanite. However,

it should be noted that our kimuraite subsamples displayed concave tetrad patterns quite analogous to other kimuraite samples in previous studies. Given that our kimuraite subsamples are mixtures, such concave tetrad pattern of kimuraite is not supposed to be discerned from our samples, due to the disturbance from lanthanite. But in fact, lanthanite itself seems to have a special REE pattern. Although Pr, Tb, Ho and Tm were not able to be measured with ID-MS, Akagi et al. (1996) suggested that lanthanite might have a concave tetrad pattern like kimuraite. Since lanthanite also holds a concave tetrad pattern like kimuraite, even though a small portion of lanthanite is present in our kimuraite samples, it will not erase the tetrad pattern of kimuraite, only causing slight compositional changes to the bulk samples.

Kimuraite and lanthanite are coexisting minerals that were contemporaneously formed from a hydrothermal fluid. The crystallization of kimuraite consumes a large amount of Y-group rare earths, and causes a dramatic decrease of these elements, together with a relative enrichment of light rare earths, to the local fluid. Immediately after the formation of kimuraite, lanthanite starts to crystallize from such a fluid.

3.6 Conclusions

Seven kimuraite subsamples have been studied in this work, but none of them exhibited the same composition with the kimuraite approved by IMA. In the BSE images of our kimuraite sample, another mineral of bright intensity was observed, and this is for the first time to report the occurrence of another mineral in the cleavage of kimuraite. Though it is impossible for us to directly measure its composition, it can be inferred from the available information that this mineral is most likely to be lanthanite. Therefore, from our finding, we should be cautious when we conduct a study on kimuraite, because there is a possibility for kimuraite to be contaminated by other mineral formed in its cleavage.

4. Applications of the improved Jørgensen equation to the REE patterns of kimuraite and lanthanite

4.1 Improved Jørgensen equation for the chondrite-normalized REE pattern

In the first chapter of this thesis, we have successfully regressed the tetrad effects in the logK_d distribution patterns of REE with the improved Jørgensen equation (4.1).

$$\log K_d = A+(a+bq)q(q+25)+(9/13)n(S)C_1(q+25)+m(L)C_3(q+25) \quad (4.1)$$

Kawabe and Masuda (2001) argued that plotting the logarithmic normalized REE values against the atomic number for geologic samples should be analogous to the logK_d pattern in thermodynamics, with regard to their intimate involvements of the thermochemical consequences of the nephelauxetic effect in Ln^{3+}. According to their suggestion, equation (4.1) can be developed into a new form which is proper for the quantitative description of tetrad effects in the logarithmic REE patters for various natural samples.

$$log(REE)_n = A+(a+bq)q(q+25)+(9/13)n(S)C_1(q+25)+m(L)C_3(q+25) \quad (4.2)$$

On the left side of equation (4.2), $log(REE)_n$ represents the logarithmic values of REE concentration ratios relative to a reference material (e.g. chondrite), which are generally classified into three types (Kawabe et al., 2012). The most familiar one is the chondrite-normalized REE concentration ratios. The second type is the REE concentration ratios between two coexisting phases. Besides these two types, there is a third one which has drawn little attention, and it is the concentration ratios between two same mineral samples collected from different places. On the right side of equation (4.2), q denotes the number of 4f electrons in [Xe](4f^q) electronic configuration of REE^{3+}. $n(S)$ and $m(L)$ are constant coefficients, whose values are given by the total spin quantum number S and the total orbital quantum number L for the ground term (^{2S+1}L) of the electronic configuration in the Russell-Saunders coupling. Although the constant coefficients, A, a, b, C_1 and C_3, will be determined by

the same method, they have different meanings from those parameters in equation (4.1).

Kawabe et al. (2008) made the attempt to use equation (4.2) to deal with the chondrite-normalized REE patterns of several basalt samples, which had been treated as tetrad effects, and showed that these tetrad effects could be reproduced by this equation with or without some empirical corrections for La and Ce. Recently, similar effort to apply equation (4.2) to the chondrite-normalized patterns of two kimuraite samples from Japan was performed by Kawabe et al. (2012), but one of them could not be regressed by equation (4.2) unless some corrections were made to the abundances of light REE, which contradicts to the proposal made by Akagi et al. (1993) that the chondrite-normalized REE pattern of this kimuraite exhibits a tetrad effect.

As to this study, we will carry on the similar efforts to apply equation (4.2) to the chondrite-normalized REE patterns of kimuraite and lanthanite, since both of them were suggested to exhibit tetrad effects (Akagi et al., 1993; Akagi et al., 1996). In addition, the REE partition between kimuraite and lanthanite, which are two co-existing REE^{3+} phases in a low-temperature hydrothermal fluid, also seems to yield a tetrad effect (Kawabe et al., 2012). Therefore, the lanthanite-normalized REE pattern of kimuraite will also be fitted by the improved Jørgensen equation.

4.2 Data compilation

In the earlier section of this thesis, we have reported the chemical compositions of seven kimuraite subsamples taken from a spherulitic aggregate of kimuraite, which was collected from the alkali olivine basalt in Hizencho, Higashi Matsuura, Saga Prefecture, Japan, and found out that this kimuraite aggregate is contaminated by a small amount of lanthanite. In this section, the average composition of seven kimuraite subsamples will be used as the composition of the aggregate kimuraite sample (Table 4.1). From the same location, other four kimuraite samples have been analyzed by previous studies (Nagashima et al., 1986; Akagi et al., 1993). The compositions of these kimuraite samples are listed in Table 4.1. At present, two lanthanite samples from Hizen-Cho have been studied by Nagashima et al. (1986) and Akagi et al. (1996), but neither of them has complete data about the REE composition. Based on the lanthanite data reported by Graham et al. (2007), Kawabe et al. (2012) estimated the abundances of four monoisotopic elements (Pr, Tb, Ho and Tm), which

(ppm)	Jiao et al. (2013)	Akagi et al. (1993)			Nagashima et al. (1986)
		middle layer kimuraite A	inner layer kimuraite A	specimen B	
La	12900 (2130)	4940	5970 (915)	5700	4270
Ce	7.71	10	13.6	27	170
Pr	4130 (2280)	3490	2690 (1200)	3860	3160
Nd	27500 (27100)	31600	19600 (12400)	31600	24900
Sm	10000	16900	7860	16300	8460
Eu	5030	8650	3880	7900	3370
Gd	28300	51700	27000	45900	21600
Tb	4090	7480	4210	7130	3160
Dy	24300	40700	25900	42800	21100
Ho	5510	7630	6220	8800	5430
Er	13600	15700	15100	20600	14800
Tm	1200	1080	1440	1650	1490
Yb	3080	3970	4880	5500	4910
Lu	366	489	614	683	532

Table 4.1. REE compositions of five kimuraite samples from Southwest Japan. In the brackets are those corrected values.

(ppm)	Seredin et al. (2009)	Nagahisma et al. (1986)	Akagi et al. (1996)	Graham et al. (2007)
La	9389	134000	151000	248000
Pr	3030	44300	(35500)	63600
Nd	13999	201000	163000	273000
Sm	2676	31800	30500	46500
Eu	516	6910	8890	12100
Gd	1864	15100	28500	32900
Tb	171	869	(2290)	2690
Dy	603	2960	5940	8190
Ho	81.0(37.9)	175	(582)	524
Er	152(40.4)	262	734	612
Tm	15.0(2.63)	(12.9)	(43)	(33.9)
Yb	73.0(6.69)	(27.7)	91.9	111
Lu	9.00(0.43)	(2.52)	8.75	11.1

Table 4.2. REE compositions of four lanthanite samples. The values in brackets are all interpolated, based on the REE composition of Graham et al. (2007).

were not able to be obtained by the isotope dilution method (Akagi et al., 1996). Similarly, the abundances of Tm, Yb and Lu, which were not provided by Nagashima

et al. (1986), have been interpolated by us (Table 4.1).

Apart from the occurrence of this carbonate REE mineral assemblage in southwest Japan, the same assemblage has also been found from the Abramovskoye ore deposit in Russia. Six kimuraite ore samples and one lanthanite ore sample were analyzed by Seredin et al. (2009), and their compositions are summarized in Table 4.2 and 4.3, respectively. At the meantime, the REE abundances of four other kimuraite samples, which were claimed to be contaminated by lanthanite, were also provided by Seredin et al. (2009) (Table 3). Their chondrite-normalized REE patterns will also be looked into with Jørgensen-Kawabe equation.

(ppm)	Kimuraite samples						Kimuraite-lanthanite samples			
	10/07	66/00	66/97	58/97	57/97	8/00	10/04	10/01	10/03	10/06
La	3700 (70.9)	316 (7.42)	118 (8.92)	233 (24.6)	188 (16.6)	144 (14.1)	1230	766	546	529
Ce	23.0	23.0	10.3	144	75.7	109	35.2	40.4	64.1	106
Pr	704 (89.1)	60.0 (8.91)	37.2 (9.77)	61.4 (17.8)	39.7 (11.0)	32.0 (8.13)	319	228	161	152
Nd	4340 (1430)	320 (98.9)	240 (103)	338 (164)	212 (99.0)	154 (65.4)	1370	978	707	663
Sm	1830	107	100	113	61.5	40.0	288	204	158	135
Eu	661	38.0	38.1	39.7	20.7	12.0	61.0	40.9	33.4	28.9
Gd	7650	439	389	378	199	110	303	181	154	126
Tb	1530	91.0	70.0	52.9	25.5	16.0	42.9	25.6	22.8	18.2
Dy	11300	724	533	345	160	95.0	252	141	136	108
Ho	2820	206	127	81.6	38.3	25.0	49.6	26.9	26.1	21.1
Er	7180	622	346	217	100	61.0	123	66.5	65.9	54.7
Tm	771	101	39.7	23.9	10.6	8.00	16.1	8.80	9.10	7.40
Yb	3140	436	203	104	44.8	31.0	84.2	45.9	50.2	40.7
Lu	372	78.0	28.4	16.9	7.2	6.00	11.7	6.40	7.00	5.70

Table 4.3. REE compositions of six kimuraite samples and four kimuraite-lanthanite samples from Abramovskoye ore deposit in Russia (Seredin et al., 2009). In the brackets are the corrected values given by us.

4.3 Results and Discussions

4.3.1 Chondrite-normalized REE patterns of lanthanite

In spite of the absence of four monoisotopic rare earth elements, the chondrite-normalized REE pattern of lanthanite was suggested to be a tetrad effect (Akagi et al., 1996). Very recently, another lanthanite was found from New Zealand

by Graham et al. (2007), with all rare earth elements but Tm being determined. This lanthanite sample was later used by Kawabe et al. (2012) to estimate the abundances of four unreported monoisotopic elements of the former lanthanite sample. Then, the chondrite-normalized REE patterns of these two lanthanite samples were further investigated with Jørgensen-Kawabe equation (Kawabe et al., 2012). As a result, both REE patterns could be reproduced by Jørgensen-Kawabe equation, which corresponded with the suggestion made by Akagi et al. (1996) that the chondrite-normalized REE pattern displays a tetrad effect.

Besides the above two lanthanite samples, there are other two lanthanite samples reported by Nagashima et al. (1986) and Seredin et al. (2009), respectively. The last

	sample	*A*	*a*	*b*	C_1	C_3
lanthanite	Nagashima et al. (1986)	5.94±0.10	(-5.27±2.90)×10^{-3}	(-1.53±2.10)×10^{-4}	(-7.57±7.73)×10^{-4}	(0.19±2.47)×10^{-4}
	Seredin et al. (2009)	4.70±0.06	(-3.48±1.60)×10^{-3}	(-2.01±1.15)×10^{-4}	(-8.73±4.26)×10^{-4}	(0.15±1.36)×10^{-4}
kimuraite from Japan	Nagashima et al. (1986)	4.25±0.05	(3.38±1.29)×10^{-3}	(-2.23±0.93)×10^{-4}	(-6.85±3.44)×10^{-4}	(-3.76±1.09×10^{-4}
	Kimuraite B (Akagi et al., 1993)	4.34±0.03	(3.88±0.85)×10^{-3}	(-2.63±0.61)×10^{-4}	(-1.25±0.23)×10^{-3}	(-3.38±0.72)×10^{-4}
	middle layer kimuraite A (Akagi et al., 1993)	4.31±0.03	(3.62±0.73)×10^{-3}	(-2.62±0.53)×10^{-4}	(-1.60±0.20)×10^{-3}	(-3.45±0.62)×10^{-4}
	inner layer kimuraite A (Akagi et al., 1993)	3.77±0.02	(5.64±0.67)×10^{-3}	(-3.18±0.48)×10^{-4}	(-1.30±0.18)×10^{-3}	(-3.47±0.57)×10^{-4}
	Jiao et al. (2013)	4.08±0.04	(4.57±1.02)×10^{-3}	(-3.18±0.73)×10^{-4}	(-1.17±0.27)×10^{-3}	(-4.11±0.87)×10^{-4}
kimuraite from Russia	10/07	3.15±0.05	(0.71±0.13)×10^{-2}	(-3.68±0.91)×10^{-4}	(-0.90±0.34)×10^{-3}	(-3.06±1.07)×10^{-4}
	66/00	1.50±0.03	(9.24±0.87)×10^{-3}	(-4.02±0.63)×10^{-4}	(-0.88±0.23)×10^{-3}	(-1.75±0.74)×10^{-4}
	66/97	1.59±0.01	(8.30±0.41)×10^{-3}	(-4.01±0.29)×10^{-4}	(-1.09±0.11)×10^{-3}	(-1.84±0.35)×10^{-4}
	58/97	2.03±0.02	(3.96±0.53)×10^{-3}	(-1.78±0.39)×10^{-4}	(-1.41±0.14)×10^{-3}	(-2.73±0.45)×10^{-4}
	57/97	1.86±0.02	(2.93±0.57)×10^{-3}	(-1.31±0.41)×10^{-4}	(-1.49±0.15)×10^{-3}	(-3.03±0.48)×10^{-4}
	8/00	1.78±0.03	(2.11±0.90)×10^{-3}	(-0.73±0.65)×10^{-4}	(-1.35±0.34)×10^{-3}	(-2.74±0.76)×10^{-4}
kimuraite-lanthanite	10/04	3.71±0.01	(-3.63±0.33)×10^{-3}	(1.26±0.24)×10^{-4}	(-1.78±0.88)×10^{-4}	(-0.67±0.28)×10^{-4}
	10/01	3.55±0.02	(-3.31±0.57)×10^{-3}	(0.86±0.41)×10^{-4}	(-0.20±1.51)×10^{-4}	(-0.18±0.48)×10^{-4}
	10/03	3.39±0.01	(-2.80±0.33)×10^{-3}	(0.78±0.24)×10^{-4}	(-0.11±0.88)×10^{-4}	(-0.12±0.28)×10^{-4}
	10/06	3.38±0.01	(-3.33±0.42)×10^{-3}	(1.05±0.30)×10^{-4}	(0.08±1.11)×10^{-4}	(-0.32±0.36)×10^{-4}

Table 4.4. The values of five parameters in Jørgensen-Kawabe equation determined by the chondrite-normalized REE values.

three rare earth elements (Tm, Yb and Lu) of the former one, which were not

determined by Nagashima et al. (1986), were interpolated by normalizing this lanthanite to that of Graham et al. (2007) (Fig. 4.1). Due to the remarkable negative anomaly, Ce was excluded from the least square method, as well as Pm. Therefore, the remaining thirteen rare earth elements were used to determine five parameters in

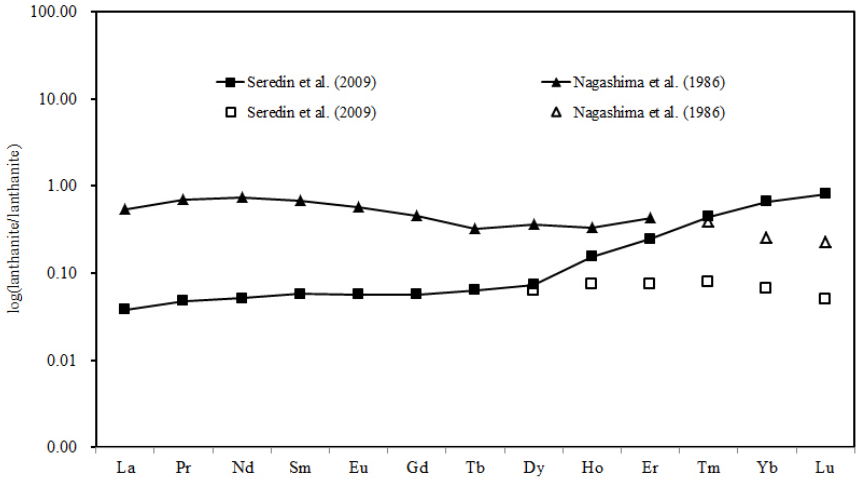

Figure 4.1. The lanthanite sample of Nagashima et al. (1986) and another one of Seredin et al. (2009) were normalized to the reference sample reported by Graham et al. (2007). Solid triangles and squares are primitive values, while hollow triangles and squares stand for the corrected values.

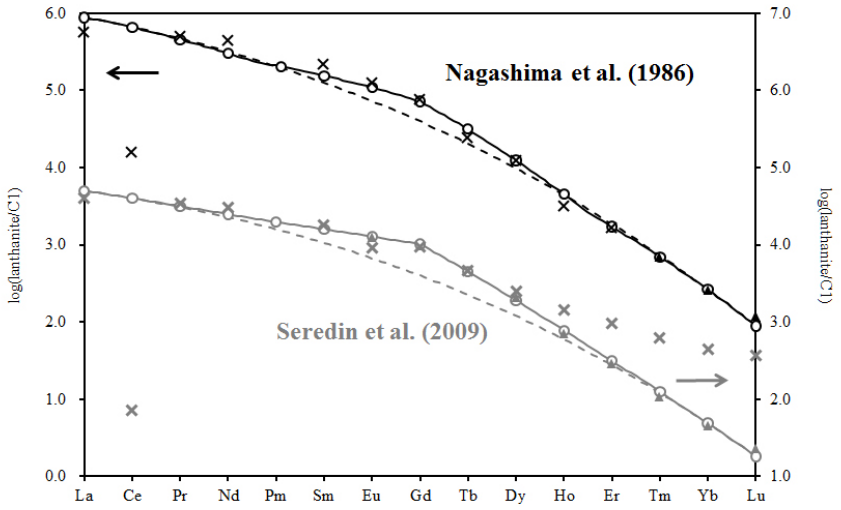

Figure 4.2. Chondrite-normalized REE patterns of two lanthanite samples and corresponding tetrad effects regressed by Jørgensen-Kawabe equation. Crosses are the primitive chondrite-normalized REE values; solid triangles represent the interpolated values; the solid lines made up of circles denote the regressed tetrad effects; the dashed lines stand for the smooth variation cross the REE series.

equation (1), namely A, a, b, C_1 and C_3. As their values are derived from least-squares

method, we can put them back into equation (1), then obtain the regressed values of log*(REE)*, which will yield a theoretical tetrad effect. In Fig. 4.2, the chondrite-normalized REE pattern of lanthanite obviously exhibits a tetrad effect, as it is identical to the regressed tetrad effect. Using the parameters determined by least-squares method (Table 4.4), this chondrite-normalized REE pattern can be described quantitatively.

Meanwhile, the same work was done to the chondrite-normalized REE pattern of the lanthanite from Russia. An unexpected result came out that Jørgensen-Kawabe equation was not able to reproduce the tetrad effect of this lanthanite immediately. When we normalized it to the reference sample, a remarkable enrichment of HREE turned up (Fig. 4.1). Considering that this lanthanite sample was collected from a REE ore deposit, it is a possible scenario that this ore sample is mixed with other HREE-rich phases (e.g. kimuraite) rather than a pure lanthanite. Therefore, proper corrections are needed to the abundances of HREE. Otherwise the chondrite-normalized REE pattern cannot be reproduced by Jørgensen-Kawabe equation (Fig. 4.2). If Seredin et al. (2009) had determined the abundance of Ca, they could have known whether this ore sample is a pure lanthanite or not through the mole ratio of Ca to REE.

In Jørgensen-Kawabe equation, $C_1(q+25)$ and $C_3(q+25)$ directly control the degree of tetrad effect. The chondrite-normalized REE patterns of these two lanthanite samples approximately show same tetrad effects, because C_1 and C_3 take similar values (Table 4.4). Masuda et al. (1987) suggested there are two types of tetrad effects in the normalized REE patterns, namely W-type and M-type. From the perspective of C_1 and C_3, W-type tetrad effect requires both C_1 and C_3 take negative values, while both positive values for C_1 and C_3 of M-type tetrad effect (Kawabe et al., 2008). As for these two lanthanite samples, both C_1 possess positive values, in comparison to the positive values of C_3. Therefore, the tetrad effect of lanthanite cannot be simply classified as W-type or M-type.

Definitely, lanthanite is not a coexisting phase with the chondrite material, and the chondrite-normalized REE pattern of lanthanite is to reveal the integral fractionation of REE. Applying Jørgensen-Kawabe equation to quantitatively describe the REE pattern offers a new way to understand the overall fractionation of REE. From chondrite material to lanthanite, it is quite certain that the fractionation of REE has already repeated for a couple of times or more. The tetrad effect recognized in chondrite-normalized REE pattern indicates that no matter how many times the REE fraction has occurred, each single step of REE fractionation is to yield a tetrad effect, which is able to be regressed by Jørgensen-Kawabe equation. As a result, those parameters, A, a, b, C_1 and C_3, used to define the tetrad effect in chondrite-normalized

REE pattern can be regarded as the sum of the corresponding parameter in each equation.

4.3.2 Chondrite-normalized REE patterns of kimuraite

The chondrite-normalized REE patterns of kimuraite showing tetrad effects was initially demonstrated by Akagi et al. (1993), where the REE compositions of three kimuraite samples (including inner layer kimuraite A, middle layer kimuraite A and kimuraite B) were studied. Still, an important fact has apparently been neglected that the REE composition of inner layer kimuraite A is much different from those of other two kimuraite samples. As two major elements, Y and Ca, were not determined, further judgment cannot be reached. In this context, Kawabe et al. (2012) examined the chondrite-normalized REE patterns of inner layer kimuraite A and middle layer kimuraite A with Jørgensen-Kawabe equation, and the result turned out to be interesting that the chondrite-normalized REE pattern of inner layer kimuraite A could not be regressed by Jørgensen-Kawabe equation immediately, while the other one was proved to show a tetrad effect. Thus, more effort is needed as we are going to make a comprehensive examination of the chondrite-normalized patterns of all kimuraite samples with Jørgensen-Kawabe equation.

Besides the above two kimuraite samples, there are other three kimuraite samples from southwest Japan to be discussed. As the chondrite-normalized REE values of the kimuraite sample of Nagashima et al. (1986) were applied to Jørgensen-Kawabe equation, five parameters could be worked out by least-squares method (Table 4.4),

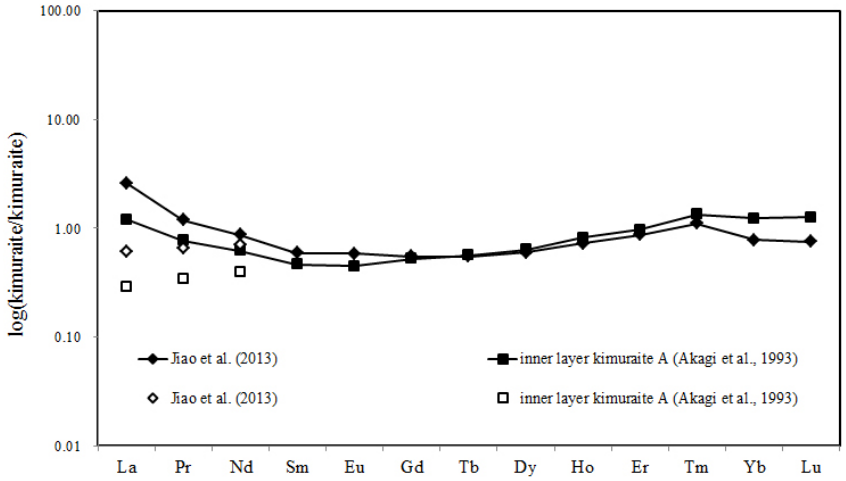

Figure 4.3. Two kimuraite samples, reported respectively by Akagi et al. (1993) and Jiao et al. (2013), were normalized to kimuraite B of Akagi et al. (1993). Solid triangles and squares are the original values, while hollow triangles and squares represent the corrected values.

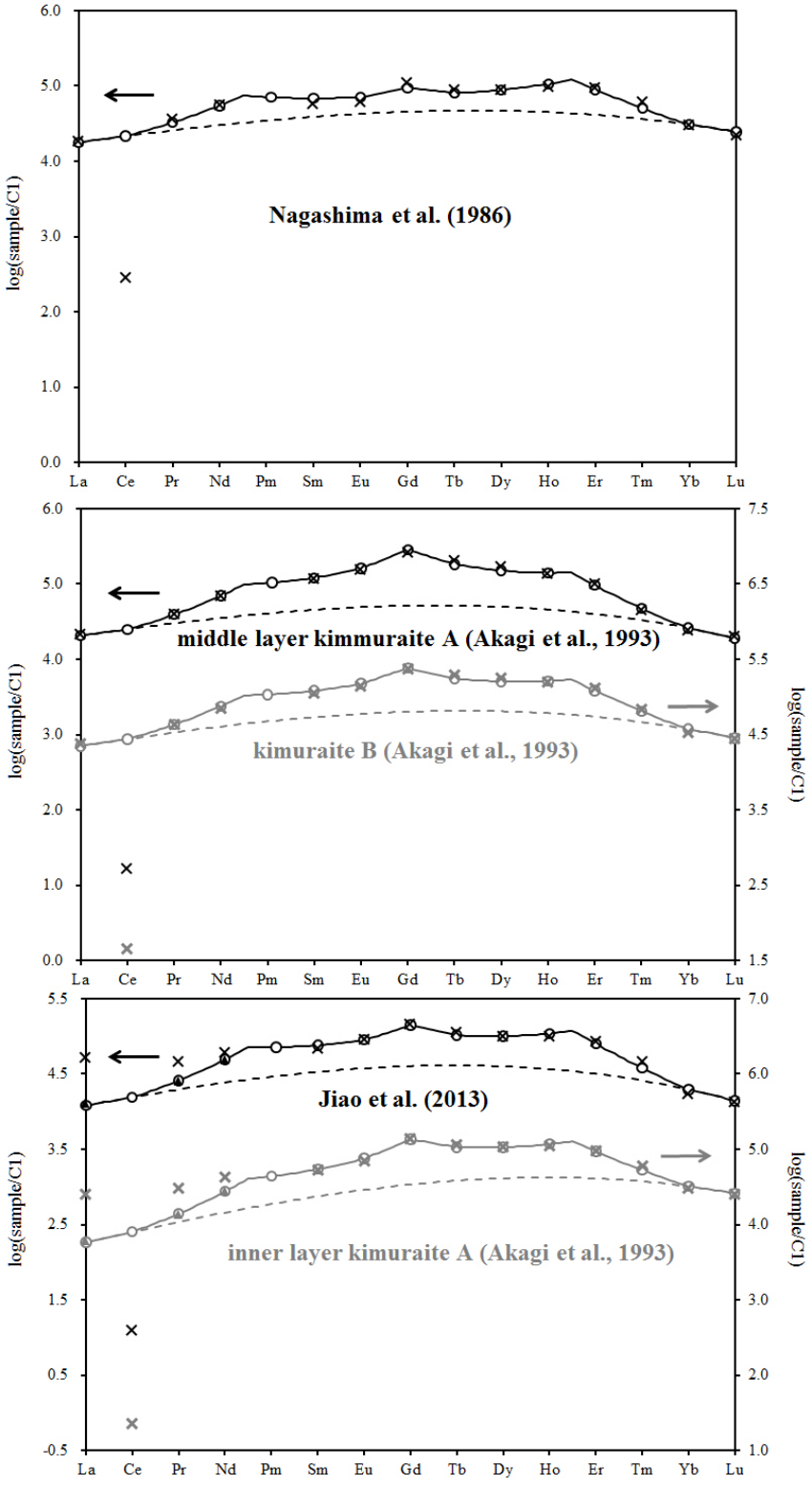

Figure 4.4. Chondrite-normalized REE patterns of five kimuraite samples from southwest Japan, and corresponding tetrad effects regressed by Jørgensen-Kawabe equation. Crosses are the primitive chondrite-normalized REE values; solid triangles represent the interpolated values; the solid lines made up of circles denote the regressed tetrad effects; the dashed lines stand for the smooth variation cross the REE series.

and the theoretical tetrad effect defined by these parameters matched the chondrite-normalized REE pattern quite well. Thus, this chondrite-normalized REE pattern has been confirmed to display a tetrad effect, and can be quantitatively expressed by Jørgensen-Kawabe equation.

At the meantime, the application of Jørgensen-Kawabe equation to kimuraite B came out with the same result that its chondrite-normalized REE pattern exhibits a tetrad effect. In comparison, the first trial to examine the chondrite-normalized REE pattern of the kimuraite reported by Jiao et al. (2013) confirmed that it was not able to be reproduced by the equation. Actually, this makes sense as this kimuraite is contaminated by lanthanite, according to Jiao et al. (2013). The abundances of HREE in lanthanite are so low, when compared to kimuraite, that the contamination of lanthanite will not introduce a significant disturbance to the overall HREE composition. Therefore, we only corrected the abundances of LREE, in order to remove the interference from lanthanite by normalizing it to kimuraite B (Fig. 4.3). As a result, the REE pattern became reproducible when the corrected values were applied to the equation (Fig. 4.4). Since this situation is nearly the same with that has already been seen in the inner layer kimuraite A (Fig. 4.4), we believe that inner layer kimuraite A is also contaminated by lanthanite. In Table 4, the tetrad effects of three kimuraite samples from southwest Japan have similar values for their parameters, and the negative values of C_1 and C_3 is responsible for the concave curves in shape, or W-type. With the help of this equation, we can quantitatively define a tetrad effect, instead of judging by the appearance, which is apt to lead to a misjudgment like Akagi et al. (1993).

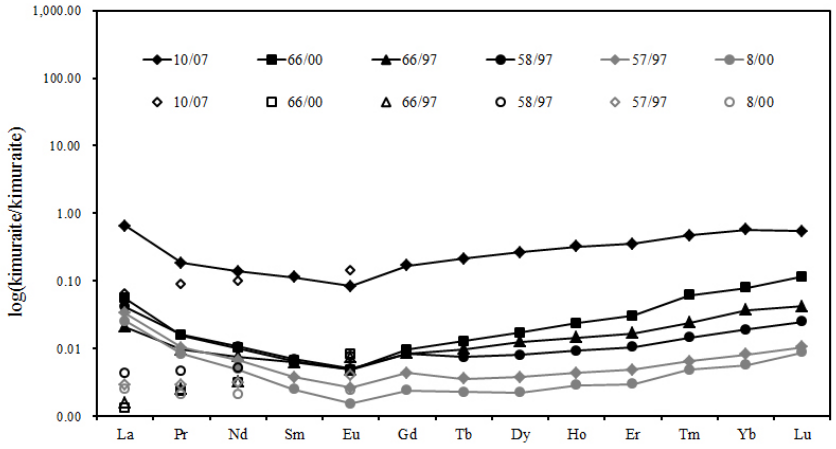

Figure 4.5. Six kimuraite samples of Seredin et al. (2009) were normalized to kimuraite B of Akagi et al. (1993). Solid triangles and squares are the original values, while hollow triangles and squares represent the corrected values.

From the REE ore deposit in Russia, Seredin et al. (2009) reported the REE compositions of six kimuraite samples and other four kimuraite-lanthanite samples were analyzed. When we applied Jørgensen-Kawabe equation to the chondrite-normalized REE patterns of these kimuraite samples, none of them could be quantitatively expressed by the equation. Like the lanthanite sample, all kimuraite samples are described as ore samples by Seredin et al (2009), giving a possibility that these kimuraite samples are not pure kimuraite. As these samples are normalized to kimuraite B, it seems that all samples have excessive amounts of LREE (Fig. 4.5). At the same time, all kimuraite ore samples show similar negative Eu anomalies, implying the existence of a LREE-rich pollutant phase in kimuraite ore samples. Hence, we empirically corrected the LREE and Eu abundances of them. As expected, all corrected REE patterns were able to be reproduced by the equation. The parameters for each tetrad effect are summarized in Table 4.4, and the chondrite-normalized REE patterns are plotted together with the regressed patterns in Fig. 4.6.

The chondrite-normalized REE patterns of two kimuraite samples from southwest Japan, which are contaminated by lanthanite, are not applicable to the equation, unless appropriate corrections are made. In the same way, it is reasonable that the chondrite-normalized REE patterns of four kimuraite-lanthanite samples reported by Seredin et al. (2009) are not able to be reproduced by Jørgensen-Kawabe equation. But in fact, all of them are immediately regressed by the equation with Ce and Eu being corrected, and characterized by faint tetrad effects (Fig. 4.7). Such an outcome obviously contradicts to what we have previously expected. These samples are labeled as kimuraite-lanthanite by Seredin et al. (2009), but neither the crystal structures nor the Ca abundances of them are reported. In our point of view, our results do not support that they are mechanical mixtures, but indicate one homogeneous phase instead. Their chondrite-normalized REE patterns are quite different from those of kimuraite and lanthanite, which can be seen from the parameters in Table 4.4. Thus, it can be inferred, at least, that this homogeneous phase is neither kimuraite nor lanthanite, and possibly represents the chemical composition of the source fluid.

By applying the chondrite-normalized REE values to Jørgensen-Kawabe equation, we can conclude that the chondrite-normalized REE pattern of kimuraite exhibits a W-type tetrad effect, since both C_1 and C_3 are negative values (Table 4). In the former study, Akagi et al. (1993), judging from the shapes, came to a conclusion that the chondrite-normalized REE patterns of three kimuraite samples are W-type tetrad effects. However, our study has disclosed that the REE pattern of inner layer kimuraite A cannot be counted as a typical tetrad effect, due to the anomaly of LREE introduced by the contamination of lanthanite. Likewise, the chondrite-normalized

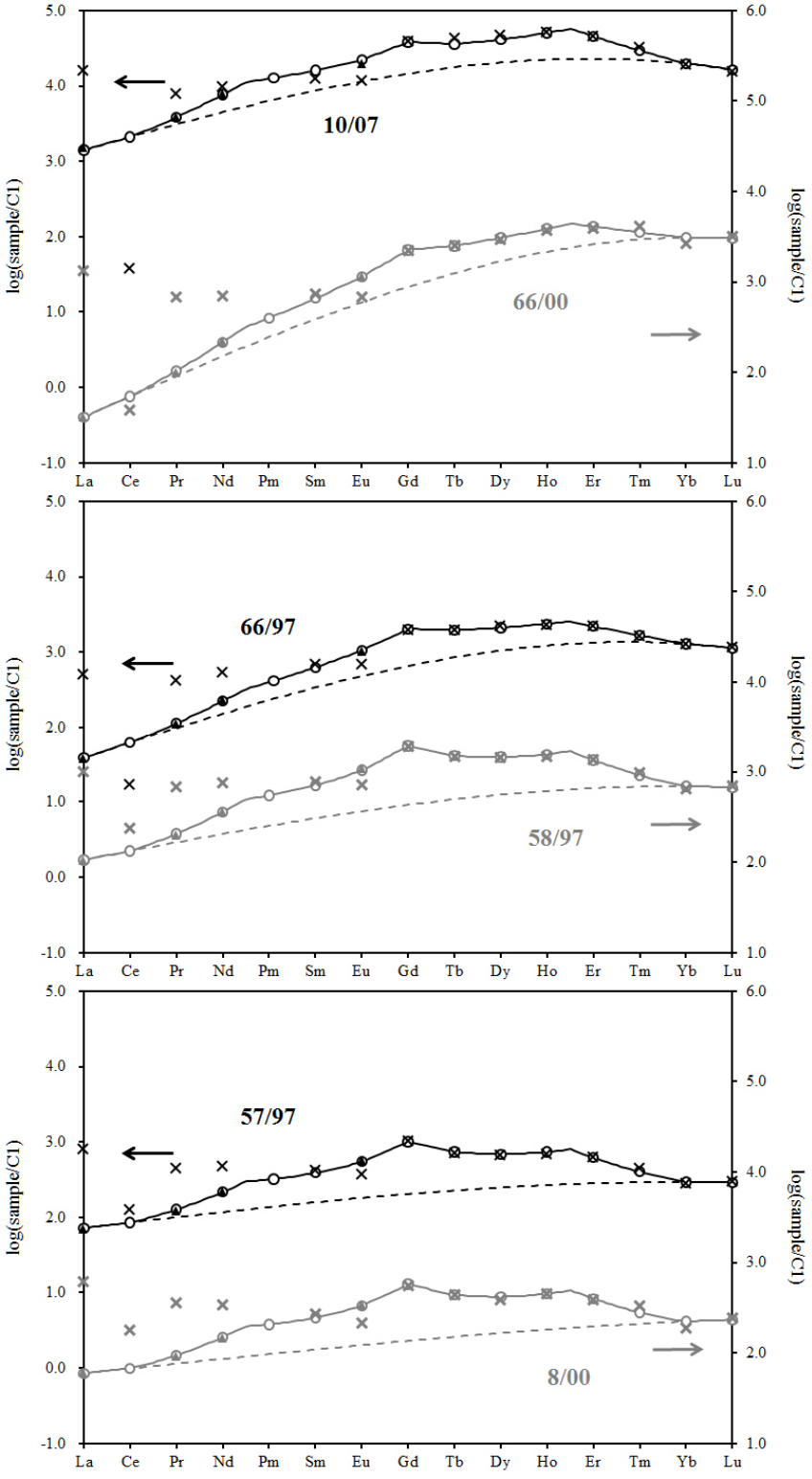

Figure 4.6. Chondrite-normalized REE patterns of six kimuraite samples from Russia, and corresponding tetrad effects regressed by Jørgensen-Kawabe equation. Crosses are the primitive chondrite-normalized REE values; solid triangles represent the interpolated values; the solid lines made up of circles denote the regressed tetrad effects; the dashed lines stand for the smooth variation cross the REE series.

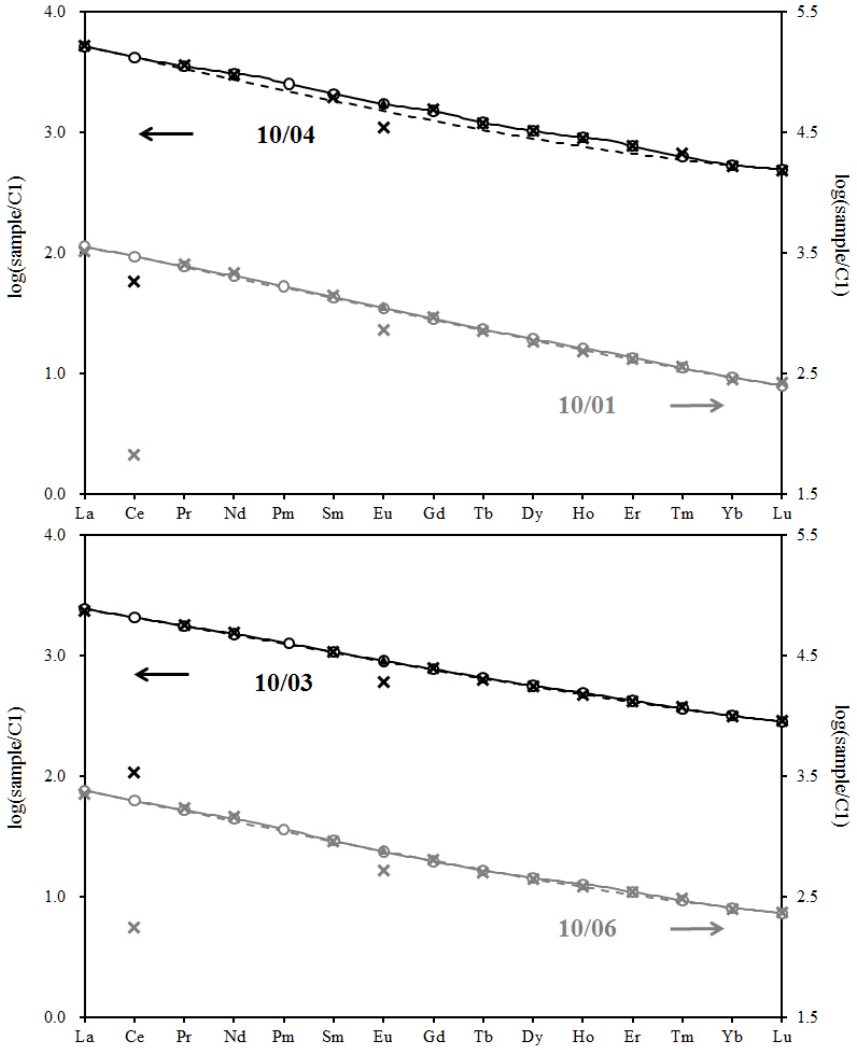

Figure 4.7. Chondrite-normalized REE patterns of four kimuraite-lanthanite samples from Russia, and corresponding tetrad effects regressed by Jørgensen-Kawabe equation. Crosses are the primitive chondrite-normalized REE values; solid triangles represent the interpolated values; the solid lines made up of circles denote the regressed tetrad effects; the dashed lines stand for the smooth variation cross the REE series.

REE patterns of kimuraite samples from Russia exhibit W-type tetrad effects in appearance. But, when they are applied to Jørgensen-Kawabe equation, it can be found that none of them exhibits a typical tetrad effect, as the same contamination has probably occurred to them. There seems to be a lot of unfavorable factors hampering the recognition of tetrad effect, and consequently, to discuss about a tetrad effect only by its appearance is not appropriate. In order to identify the tetrad effect properly, the Jørgensen-Kawabe equation should be used.

4.3.3 REE fractionation between two coexisting phases

Kimuraite and lanthanite are considered as a coexisting mineral pair, which is simultaneously precipitated from a CO_2-rich fluid, and their formation temperature is estimated to be around 150℃ (Seredin et al., 2009). The REE partitioning between these two minerals, to a certain extent, is much analogous to the situation where REE partitioning between two coexisted phases in chemical systems (Davranche et al., 2005). Recently, Kawabe et al. (2012) studied the lanthanite-normalized REE patterns of middle layer kimuraite A and inner layer kimuraite A reported by Akagi et al. (1993), and found out that the former could be reproduced by Jørgensen-Kawabe equation while the latter failed due to the excessive amount of LREE. In earlier discussions of this paper, the excessive amount of LREE has been ascribed to the contamination of lanthanite. Like inner layer kimuraite A, other seven kimuraite

	sample	*A*	*a*	*b*	C_1	C_3
kimuraite from Japan	Nagashima et al. (1986)	-1.59±0.06	(9.41±1.62)×10^{-3}	(-2.17±1.17)×10^{-4}	(8.35±4.31)×10^{-4}	(-2.03±1.37)×10^{-4}
	Kimuraite B (Akagi et al., 1993)	-1.50±0.04	(9.91±1.12)×10^{-3}	(-2.60±0.81)×10^{-4}	(2.70±2.98)×10^{-4}	(-1.60±0.95)×10^{-4}
	middle layer kimuraite A (Akagi et al., 1993)	-1.53±0.03	(9.65±0.92)×10^{-3}	(-2.56±0.66)×10^{-4}	(-0.80±2.45)×10^{-4}	(-1.72±0.78)×10^{-4}
	inner layer kimuraite A (Akagi et al., 1993)	-2.07±0.03	(1.17±0.09)×10^{-2}	(-3.10±0.68)×10^{-4}	(2.24±2.51)×10^{-4}	(-1.70±0.80)×10^{-4}
	Jiao et al. (2013)	-1.76±0.03	(1.06±0.11)×10^{-2}	(-3.1±0.81)×10^{-4}	(3.52±2.98)×10^{-4}	(-2.40±0.95)×10^{-4}
Kimuraite from Russia	10/07	-2.70±0.06	(1.31±0.16)×10^{-2}	(-3.61±1.16)×10^{-4}	(6.23±4.29)×10^{-4}	(-1.32±1.37)×10^{-4}
	66/00	-4.34±0.03	(1.53±0.07)×10^{-2}	(-3.95±0.53)×10^{-4}	(6.40±1.94)×10^{-4}	(-0.10±0.62)×10^{-4}
	66/97	-4.26±0.03	(1.43±0.08)×10^{-2}	(-3.94±0.59)×10^{-4}	(4.64±2.17)×10^{-4}	(-0.10±0.69)×10^{-4}
	58/97	-3.82±0.03	(1.00±0.08)×10^{-2}	(-1.72±0.54)×10^{-4}	(1.16±2.01)×10^{-4}	(-1.00±0.64)×10^{-4}
	57/97	-3.99±0.03	(0.90±0.08)×10^{-2}	(-1.24±0.61)×10^{-4}	(0.32±2.23)×10^{-4}	(-1.29±0.71)×10^{-4}
	8/00	-4.07±0.03	(0.82±0.08)×10^{-2}	(-0.67±0.60)×10^{-4}	(1.73±2.22)×10^{-4}	(-1.00±0.71)×10^{-4}
Kimuraite-lanthanite	10/04	-2.13±0.04	(0.24±0.10)×10^{-2}	(1.32±0.74)×10^{-4}	(1.34±0.27)×10^{-3}	(1.06±0.87)×10^{-4}
	10/01	-2.29±0.03	(0.27±0.08)×10^{-2}	(0.92±0.55)×10^{-4}	(1.50±0.20)×10^{-3}	(1.56±0.65)×10^{-4}
	10/03	-2.46±0.03	(0.32±0.08)×10^{-2}	(0.84±0.60)×10^{-4}	(1.51±0.22)×10^{-3}	(1.61±0.71)×10^{-4}
	10/06	-2.47±0.03	(0.27±0.09)×10^{-3}	(1..11±0.62)×10^{-4}	(1.52±0.23)×10^{-3}	(1.41±0.73)×10^{-4}

Table 4.5. The values of five parameters in Jørgensen-Kawabe equation determined by the lanthanite-normalized REE values.

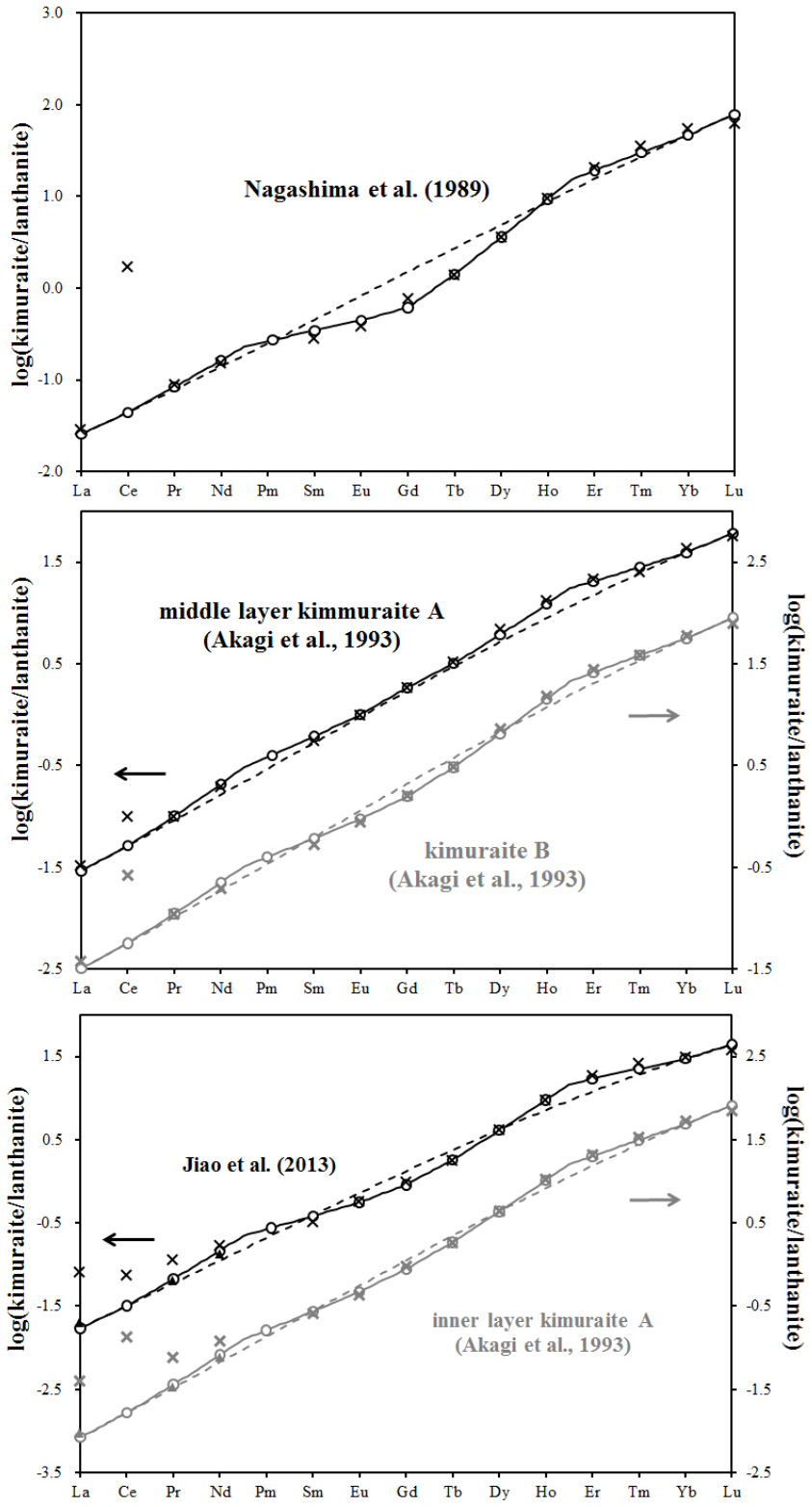

Figure 4.8. Lanthanite-normalized REE patterns of five kimuraite samples from southwest Japan, and corresponding tetrad effects regressed by Jørgensen-Kawabe equation. Crosses are the primitive chondrite-normalized REE values; solid triangles represent the interpolated values; the solid lines made up of circles denote the regressed tetrad effects; the dashed lines stand for the smooth variation cross the REE series.

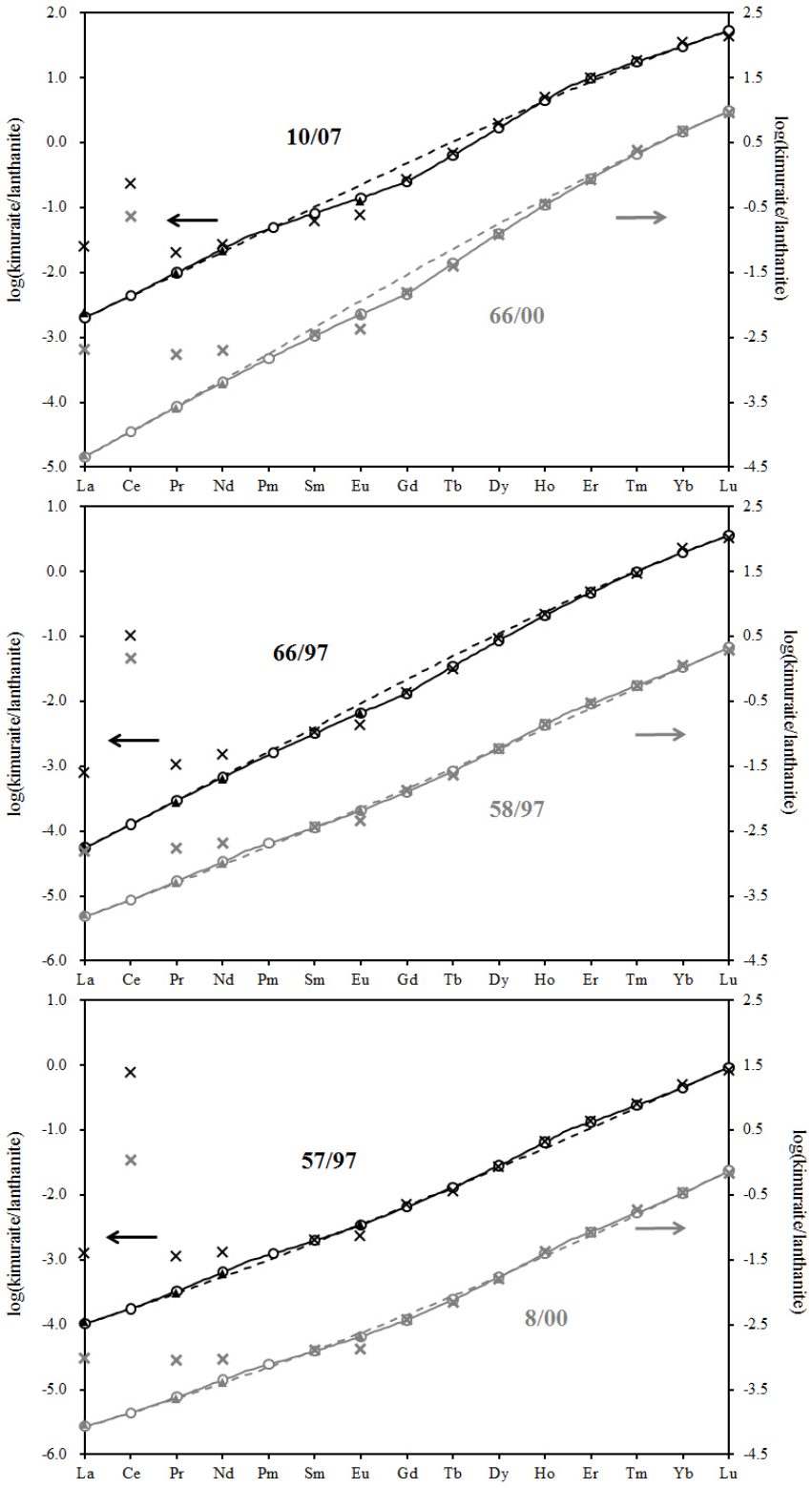

Figure 4.9. Lanthanite-normalized REE patterns of six kimuraite samples from Russia, and corresponding tetrad effects regressed by Jørgensen-Kawabe equation. Crosses are the primitive chondrite-normalized REE values; solid triangles represent the interpolated values; the solid lines made up of circles denote the regressed tetrad effects; the dashed lines stand for the smooth variation cross the REE series.

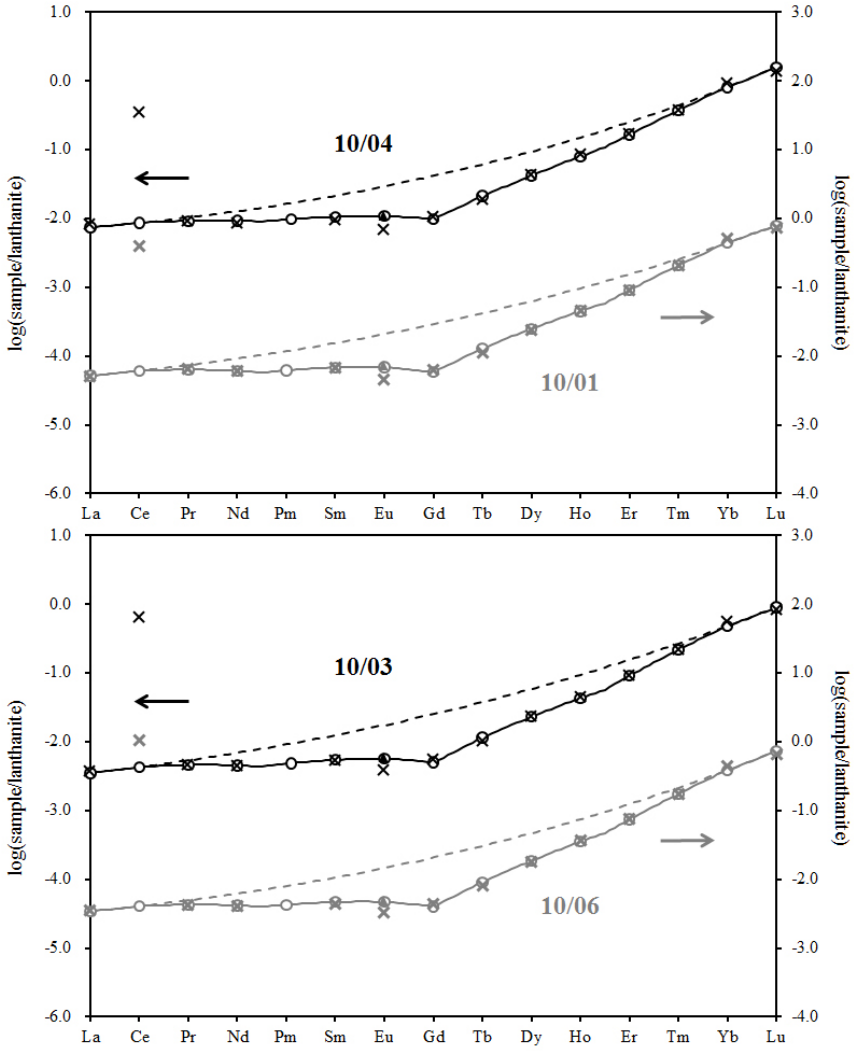

Figure 4.10. Lanthanite-normalized REE patterns of four kimuraite-lanthanite samples from Russia, and corresponding tetrad effects regressed by Jørgensen-Kawabe equation. Crosses are the primitive chondrite-normalized REE values; solid triangles represent the interpolated values; the solid lines made up of circles denote the regressed tetrad effects; the dashed lines stand for the smooth variation cross the REE series.

samples, including the kimuraite of Jiao et al. (2013) and six kimuraite of Seredin et al. (2009), are also considered to be contaminated by lanthanite. When they are normalized the lanthanite sample reported by Akagi et al. (1996), their lanthanite-normalized REE patterns are not able to be reproduced by the equation without appropriate corrections (Fig. 4.8 and 4.9). In comparison, the lanthanite-normalized REE patterns of rest three kimuraite samples are reproduced by Jørgensen-Kawabe equation, which means the REE^{3+} partitioning between kimuraite and lanthanite can yield a faint tetrad effect, and the parameters for each tetrad effect are summarized in Table 4.5. In the earlier chapter, the chondrite-normalized REE patterns of four kimuraite-lanthanite samples from Russia have been reproduced by

the theoretical equation. In Fig. 4.10, their lanthanite-normalized REE patterns again can be immediately regressed by Jørgensen-Kawabe equation, confirming that they are not mixtures.

Since the REE^{3+} partitioning between kimuraite and lanthanite is much analogous to the ligand-ligand extraction experiments of REE^{3+} performed by Peppard et al. (1969), a similar ligand exchange reaction of REE^{3+} between lanthanite [$REE_2(CO_3)_3{\cdot}8H_2O$] and kimuraite [$CaREE_2(CO_3)_4{\cdot}6H_2O$] was described by Kawabe et al. (2012), in order to illustrate the origin of tetrad effect between this natural coexisting pair of REE^{3+} species.

$$REE_2(CO_3)_3{\cdot}8H_2O(ss) + Ca^{2+}(aq) + CO_3^{2-}(aq) \rightleftharpoons CaREE_2(CO_3)_4{\cdot}6H_2O(ss) + 2H_2O(l) \quad (2)$$

The change in Gibbs free energy ΔG_r for reaction (2) can be written as below.

$$\Delta G_r = \Delta G_f^o(REE, kimuraite) - \Delta G_f^o(REE, lanthanite) + 2\Delta G_f^o(H_2O, l) - \Delta G_f^o(Ca^{2+}, aq) - \Delta G_f^o(CO_3^{2-}, aq) \quad (3)$$

As reaction (2) reaches equilibrium, ΔG_r can also be expressed by the equilibrium constant K for this reaction.

$$\Delta G_r = -2.303RT \log K \quad (4)$$

On the other hand, the equilibrium constant K is generally defined by the activities a

$$K = \frac{a(REE, kimuraite)}{a(REE, lanthanite)} \cdot \frac{a^2(H_2O, l)}{a(Ca^{2+}, aq) \cdot a(CO_3^{2-}, aq)} \quad (5)$$

$$\begin{aligned} \log K &= \log \frac{a(REE, kimuraite)}{a(REE, lanthanite)} + \log \frac{a^2(H_2O, l)}{a(Ca^{2+}, aq) \cdot a(CO_3^{2-}, aq)} \\ &= -[\Delta G_f^o(REE, kimuraite) - \Delta G_f^o(REE, lanthanite) + 2\Delta G_f^o(H_2O, l) - \Delta G_f^o(Ca^{2+}, aq) - \Delta G_f^o(CO_3^{2-}, aq)] / (2.303RT) \end{aligned} \quad (6)$$

of all chemical species which participate in the reaction. Combining equation (3) and (5), we can obtain equation (6). When a particular REE is specified in equation (6), except for the terms concerning kimuraite and lanthanite, all other terms in equation (6) can be treated as a constant. Thus, equation (6) can be written in the following

$$\log \frac{a(REE, kimuraite)}{a(REE, lanthanite)} = -[\Delta G_f^o(REE, kimuraite) - \Delta G_f^o(REE, lanthanite)] / (2.303RT) + \alpha \quad (7)$$

form, where α denotes a constant. Furthermore, the activity for a specific REE has a

$$\frac{a(REE,kimuraite)}{a(REE,lanthanite)}=\beta\cdot\frac{c(REE,kimuraite)}{c(REE,lanthanite)} \tag{8}$$

linear relationship with its mole fraction, which otherwise can be expressed by its weight concentration c. In equation (8), the linear relationship is defined by β, which is assumed to be the same across the REE series. As a consequence, equation (7) can be further transformed into equation (9)， where α^* represents (α–logβ).

$$\begin{aligned}\log\frac{c(REE,kimuraite)}{c(REE,lanthanite)}&=-[\Delta G_f^o(REE,kimuraite)-\Delta G_f^o(REE,lanthanite)]/(2.303RT)+\alpha^*\\&=[\Delta G_f^o(REE,lanthanite)-\Delta G_f^o(REE,kimuraite)]/(2.303RT)+\alpha^*\end{aligned} \tag{9}$$

Through equation (9), the logarithmic values of REE concentration ratios between kimuraite and lanthanite is connected to the change in Gibbs free energy ΔG_r for reaction (2), and the tetrad effect in lanthanite-normalized REE pattern in turn means that the variation of ($-\Delta G_r$) exhibits a tetrad effect.

As we have already known, the origin of tetrad effect is the inter-electron repulsion energy of 4f electrons. In order to illustrate the relationship between the tetrad effect in REE pattern and the inter-electron repulsion energy, we would like to develop equation (9) to the following form.

$$\begin{aligned}\log\frac{c(REE,kimuraite)}{c(REE,lanthanite)}=&[\Delta H_f^o(REE,lanthanite)-\Delta H_f^o(REE,kimuraite)]/(2.303RT)\\&+[\Delta S_f^o(REE,lanthanite)-\Delta S_f^o(REE,kimuraite)]/(2.303R)+\alpha^*\end{aligned} \tag{10}$$

Like $[\Delta G_f^o(REE,lanthanite)-\Delta G_f^o(REE,kimuraite)]$, $[\Delta H_f^o(REE,lanthanite)-\Delta H_f^o(REE,kimuraite)]$ and $[\Delta S_f^o(REE,lanthanite)-\Delta S_f^o(REE,kimuraite)]$ in equation (10) are essential parts of ΔH_r and ΔS_r for reaction (2), respectively. Therefore, the logarithmic values of REE concentration ratios are further linked with ΔH_r and ΔS_r. After an elaborate study on the thermodynamic data for $LnCl_3\cdot 6H_2O$ and $LnES_3\cdot 9H_2O$, Kawabe (1999) suggested that ΔS_r for the ligand reaction of REE^{3+} also displays a similar tetrad effect to ΔH_r, and always hinders ΔG_r from inheriting the tetrad effect in ΔH_r through the following

$$\Delta G_r=\Delta H_r-T\Delta S_r \tag{11}$$

relationship. Only when the reaction temperature is low enough, the tetrad effect in ΔG_r is approximately equal to that in ΔH_r.

The coordination number of REE^{3+} in lanthanite has been suggested to be ten by Negro et al. (1977). In comparison, the coordination state of REE^{3+} in kimuraite has not been studied yet. Since the lanthanite-normalized REE pattern of kimuraite has been successfully reproduced by Jørgensen-Kawabe equation, all REE^{3+} in kimuraite should also take a same coordination number. Otherwise, the unilateral change in coordination number of REE^{3+} in kimuraite would bring an additional disturbance to the tetrad effect, which cannot be accounted for by Jørgensen-Kawabe equation (Kawabe, 1999). Meanwhile, according to Miyawaki et al. (1993), kimuraite is structurally related to tengerite-(Y) [$Y_2(CO_3)_3 \cdot 2\text{-}3H_2O$], in which Y is 9-fold coordination. Thus, it seems that all REE^{3+} ions in kimuraite may occupy the same structural sites and take a same coordination number of 9. Consequently, the REE^{3+} ions in lanthanite are supposed to have relatively greater Racah parameters (E^1 and E^3), when compared with kimuraite. As a result, the minor differences of Racah parameters (ΔE^1 and ΔE^3) for REE^{3+} between lanthanite and kimuraite could be positive, which can cause a small M-type tetrad effect in the variation of 4f electronic configuration energy difference for REE^{3+} (Kawabe et al., 2008). According to Kawabe (1992), this type of energy difference for REE^{3+} makes an important contribution to the difference in the standard-state enthalpy of formation between lanthanite and kimuraite, namely [$\Delta H_f^o(REE,lanthanite)$-$\Delta H_f^o(REE,kimuraite)$] in equation (10). Then, the latter is expected to display an M-type tetrad effect.

In our study, we have confirmed that the lanthanite-normalized REE patterns of three kimuraite samples display faint tetrad effects (Fig. 4.8, 9, 10). Two kimuraite samples, including the kimuraite reported by Nagashima et al. (1986) and the kimuraite B reported by Akagi et al. (1993), have positive values for C_1, which is responsible for the convex octad effect. The negative values for C_3 correspond with the concave cusps at the 1/4- and the 3/4-filled 4f subshell. The positive C_1 values are in accordance with our expectation that the REE^{3+} in lanthanite have relatively larger E^1 than those in kimuraite, while the negative C_3 values seem to contradict to our expectation. Generally, Racah parameters E^1 and E^3 are likely to change coherently, and the ratio of $\Delta E^3/\Delta E^1$ (or C_3/C_1) would be kept as a constant 0.23±0.02 (Kawabe and Masuda, 2001). However, the REE^{3+} ions in kimuraite and lanthanite are coordinated with H_2O and $(CO_3)^{2-}$, and the difference in their coordination numbers is possibly very small. Only slight differences in Racah parameters (ΔE^1 and ΔE^3) for these two types of REE^{3+} could be expected. Therefore, it is possible that the difference in E^3 do not show parallel change to that in E^1. In addition, the formation temperature for kimuraite is estimated to be around 433K (Coimbra et al., 1989; Seredin et al., 2009), such a reaction temperature seems to suggest that the negative contribution from $T\Delta S_r$ cannot be ignored, resulting in a modification to the tetrad

effect for ΔH_r.

The application of Jørgensen-Kawabe equation to the REE distribution pattern between a natural mineral pair can helps us to make certain interpretations of the thermodynamic properties of the REE^{3+} ions in kimuraite and lanthanite. However, these interpretations should be treated cautiously. At present, the crystal structure of kimuraite and the thermodynamic data regarding ΔS^o and ΔH_f^o for lanthanite and kimuraite are not available. Yet, the Racah parameters for REE^{3+} in lanthanite and kimuraite have not been reported by any spectroscopic study.

4.4 Conclusions

Our study has confirmed that the chondrite-normalized REE patterns for kimuraite and lanthanite exhibit tetrad effects, and that they can be immediately reproduced by Jørgensen-Kawabe equation. With the help of this equation, we also found that the inner layer kimuraite A reported by Akagi et al. (1993) and six kimuraite samples reported by Seredin et al. (2009) are possibly contaminated by lanthanite, like our kimuraite sample. Other four samples, which were described as mixtures of kimuraite and lanthanite by Seredin et al. (2009), also had their chondrite-normalized REE patterns reproduced by Jørgensen-Kawabe equation, indicating that they might represent the REE compositions of a certain homogeneous phase rather than such mineral mixtures. Apart from the chondrite-normalized REE patterns, we also studied the REE distribution patterns between kimuraite and lanthanite, and again confirmed they exhibit faint tetrad effects, which can be accounted for from the thermodynamic viewpoint.

Being different from the single step of REE fractionation between two coexistent phases, for example kimuraite and lanthanite, the chondrite-normalized REE pattern represents the integral REE fractionation from chondrite materials to kimuraite (or lanthanite), which are absolutely not a coexisting pair. However, our efforts proved Jørgensen-Kawabe equation is also applicable to the chondrite-normalized REE pattern. From chondrite materials to kimuraite, a couple of successive REE fractionations or more have occurred. Like the REE partitioning between kimuraite and lanthanite, the REE distribution pattern in every single step of fractionation is expected to be reproducible by this theoretical equation, and to display a tetrad effect. As a result, the chondrite-normalized REE pattern is also reproducible by Jørgensen-Kawabe equation, since the parameters for each tetrad effect are additive.

References

Albarède, F., Luais, B., Fitton, G., Semet, M., Kaminski, E., Upton, B.G.J., Bachèlery, P. and Cheminée, J.L. (1997) The geochemical regimes of Piton de la Fournaise Volcano (Réunion) during the last 530000 years. J. Petrology. 38(2), 171-201.

Anders, E. and Grevesse, N. (1989) Abundances of the elements: Meteoritic and solar Geochimica et Cosmochimica Acta, 53, 197-214.

Akagi, T., Shabani, M., Masuda, A. (1993) Lanthanide tetrad effect in kimuraite [$CaY_2(CO_3)_4 \bullet 6H_2O$]: implication of a new geochemical index. Geochimica et Cosmochimica Acta, 57, 2899-2905.

Akagi, T., Nakai, S., Shimizu, H., Masuda, A. (1996) Constraint on the geochemical stage causing tetrad effect in kimuraite: comparative studies on kimuraite and its related rocks, from REE pattern and Nd isotope ratio. Geochemical Journal, 30, 139-148.

Atencio, D., Bevins, R. E., Fleischer, M., Williams, C. T., Williams, P. A. (1989) Revision of the lanthanite group and new data from specimens from Bastnäs, Sweden and Bethlehem, USA. Mineral. Mag. 53, 639-642.

Bailey, D. K. (1993) Carbonate magmas. Journal of Geological Society London. 150, 637-651.

Bau, M. (1996) Controls on the fractionation of isovalent trace elements in magmatic and aqueous systems: evidence from Y/Ho, Zr/Hf, and lanthanide tetrad effect. Contrib. Mineral. Petrol., 123, 323-333.

Bau, M. (1997) The lanthanide tetrad effect in highly evolved felsic igneous rocks- a reply to the comment by Y. Pan. Contrib. Mineral. Petrol., 128, 409-412.

Beattie, P. (1994) Systematics and energetics of trace-element partitioning between olivine and silicate melts: implications for the nature of mineral/melt partitioning. Chem. Geol. 117, 57-71.

Belousova, E., Griffin, W., O'Reilly, S.Y. and Fisher, N. (2002) Igneous zircon: trace element composition as an indicator of source rock type. Contributions to Mineralogy and Petrology. 143(5), 602-622.

Bence, A. E. and Albee, A. L. (1968) Empirical correction factors for the electron microanalysis of silicate and oxides. Journal of Geology, 76, 382-403.

Bevins, R. E., Rowbotham, G., Stephens, F. S., Turgoose, S., Williams, P. A. (1985) Lanthanite-(Ce), $(Ce,La,Nd)_2(CO_3)_3 8H_2O$, a new mineral from Wales, U.K. American Mineralogist, 70, 411-413.

Blundy, J. and Wood, B. (1994) Prediction of crystal-melt partition coefficients from elastic moduli. Nature. 372, 452-454.

Carnall, W. T., Fields, P. R. and Rajnak, K. (1968a) Electronic energy levels in the trivalent lanthanide aquo ions, I, Pr^{3+}, Nd^{3+}, Pm^{3+}, Sm^{3+}, Dy^{3+} Ho^{3+}, Er^{3+}, and Tm^{3+}. J. Chem. Phys. 49, 4424-4442.

Carnall, W. T., Fields, P. R. and Rajnak, K. (1968b) Electronic energy levels in the trivalent lanthanide aquo ions, Ⅱ, Gd^{3+}. J. Chem. Phys. 49, 4443-4446.

Carnall, W. T., Fields, P. R. and Rajnak, K. (1968c) Electronic energy levels in the trivalent lanthanide aquo ions, Ⅲ, Tb^{3+}. J. Chem. Phys. 49, 4447-4449.

Carnall, W. T., Fields, P. R. and Rajnak, K. (1968d) Electronic energy levels in the trivalent lanthanide aquo ions, IV, Eu^{3+}. J. Chem. Phys. 49, 4450-4455.

Cesbron, F., Sichère, M. C., Vachey, H., Cassedanne, J. P., Cassedanne, J. O. (1979) La lanthanite à europium de Curitiba, Paraná, Brésil. Bull. Minéral., 102, 342-347.

Chauvel, C. and Hemond, C. (2000) Melting of a complete section of recycled oceanic crust: Trace element and Pb isotopic evidence from Iceland. Geochemistry Geophysics Geosystems. 1(2), 1001-1021.

Coimbra, A.M., Coutinho, J.M.V., Atencio, D., Iwanuch, W. (1989) Lanthanite-(Nd) from Santa Isabel, State of São Paulo: second Brazilian and world occurrence. Canadian Mineralogist, 27, 119-123.

Cotton, S. (2006) Lanthanide and actinide chemistry. Published by John Wiley & Sons, Ltd.

Dautria, J. M., Dupuy, C., Takherist, D. and Dostal, J. (1992) Carbonate metasomatism in the lithospheric mantle: peridotitic xenoliths from a melilititic district of the Sahara basin. Contrib. Mineral. Petrol. 111, 37-52.

Davranche, M., Pourret, O., Gruau, G., Dia, A., Coz-Bouhnik, M. (2005) Adsorption of REE(III)-humate complexes onto MnO_2: Experimental evidence for cerium anomaly and lanthanide tetrad effect suppression. Geochimica et Cosmochimica Acta, 69(20), 4825-4835.

Denbigh, K. (1981) The principles of chemical equilibrium. 4th ed., Cambridge Univ. Press, London, 494.

Dupuy, C., Liotard, J. M. and Dostal, J. (1992) Zr/Hf fractionation in intraplate basaltic rocks: Carbonate metasomatism in the mantle source. Georhimica et Cosmochimica Acta. 5(6), 2411-2423.

Fraga, S. and Karwowski, J. (1974) Tables of Hatree-Fock Atomic Data. The University of Alberta.

Fidelis, I. and Siekierski, S. (1966) The regularities in stability constants of some rare earth complexes. J. Inorg. Nucl. Chem., 28, 185.

Fidelis, I. and Siekierski, S. (1971) On the regularities or tetrad effect in complex formation by f-electron elements, a double-double effect. J. Inorg. Nucl. Chem., 33, 3191-3194.

Goldschmidt, V. M. (1937) The principles of distribution of chemical elements in minerals and rocks. J. Chem. Soc. 655-673.

Graham, I. T., Pogson, R. E., Colchester, D.M., Hergt, J., Martin, R. (2007) Pink lanthanite-(Nd) from Whitianga Quarry, Coromandel Peninsula, New Zealand. Canadian Mineralogist, 45, 1389-1396.

Greenwood, N. N. and Earnshaw, A. (1997) Chemistry of the Elements (second edition). Butterworth-Heinemann. 1230-1242.

Habenschuss, A. and Spedding, F. H. (1980) The coordination (hydration) of rare earth ions in aqueous chloride solutions from X-ray diffraction. Ⅲ. $SmCl_3$, $EuCl_3$ and series behavior. J. Chem. Phys. 73, 442-450.

Harmer, R. E. and Gittins J. (1998) The Case for Primary, Mantle-derived Carbonatite Magma. J. Petrology. 39(11-12), 1895-1903.

Hawkesworth, C. J., Kempton, P. D., Rogers, N. W., Ellam, R. M. and Calsteren, P. W. (1990) Continental mantle lithosphere, and sallow level enrichment processes in the earth' mantle. Earth Planet. Sci. Lett. 96, 256-268.

Irber, W. (1999) The lanthanide tetrad effect and its correlation with K/Rb, Eu/Eu*, Sr/Eu, Y/Ho, and Zr/Hf of evolving peraluminous granite suites. Geochimica et Cosmochimica Acta, 63, 489-508.

Johnson, D. A. (2006) Inter-electron repulsion and irregularity in the chemistry of transition series. Inorganic Chemistry in FocusⅢ.

Jørgensen, C. K. (1962) Electron transfer spectra of lanthanide complexes. Mol. Phys., 5, 271-277.

Jørgensen, C. K. (1979) Theoretical chemistry of rare earths. In: Handbook on the Physics and Chemistry of Rare Earths (eds, Gschneider, K. A. Jr. and L. Eyring), 3, 111-169, North-Holland, Amsterdam.

Kato, T. (2005) New accurate Bence-Albee α-factors for oxides and silicates calculated from the PAP correction procedure. Geostandards and Geoanalytical Research, 29, 83-94.

Kawabe, I. (1999a) Thermochemical parameters for solution of lanthanide(III) ethylsulphate and trichloride hydrate series: Evidence for tetrad effect and hydration change in aqua Ln^{3+} ion series. Geochemical Journal, 33, 249-265.

Kawabe, I. (1999b) Hydration change of aqueous lanthanide ions and tetrad effects in lanthanide(Ⅲ)-carbonate complexation. Geochemical Journal, 33, 267-275.

Kawabe, I. (1992) Lanthanide tetrad effect in the Ln^{3+} ionic radii and refined spin-pairing energy theory. Geochemical Journal, 26, 309-335.

Kawabe, I. and Masuda, A. (2001) The original examples of lanthanide tetrad effect in solvent extraction: A new interpretation compatible with recent progress in REE geochemistry. Geochemical Journal, 35, 215-224.

Kawabe, I., Ohta, A., Ishii, S., Tokumura, M., Miyauchi, K. (1999) REE partitioning between Fe-Mn oxyhydroxide precipitates and weakly acid NaCl solutions: Convex tetrad effect and fractionation of Y and Sc from heavy lanthanides. Geochemical Journal, 33, 167-179.

Kawabe, I., Tanaka, K, Takahashi, T. and Minagawa, T. (2008) Evidence for lanthanide tetrad effect in mafic volcanic rocks; Concave tetrad effects in REE patterns for MORB and alkali olivine basalt in western Kyushu, Japan. J. Earth Planet. Sci. Nagoya Uiniv., 55, 1-21.

Kawabe, I., Toriumi, T., Ohta, A., Miura, N. (1998) Monoisotopic REE abundances in seawater and the

origin of seawater tetrad effect. Geochemical Journal, 32, 213-229.

Keppler, H. (1993) Influence of fluorine on the enrichment of high field strength trace elements in granitic rocks. Contributions to Mineralogy and Petrology. 114(4), 479-488.

Kogarko, L. N., Henderson, C. M. B. and Pacheco, H. (1995) Primary Ca-rich carbonatite magma and carbonate-silicate-sulphide liquid immiscibility in the upper mantle. Contrib. Mineral. Petrol. 121, 267-274.

Lee, W. J. and Wyllie, P. J. (1994) Experimental data bearing on liquid immiscibility, crystal fraction, and the origin of calciocarbonatite and natrocarbonatites. Internationl Geological Review. 36, 797-819.

Little, E. J. and Mark, M. J. (1960) A complete table of electronegativities. J. Chem. Educ. 37(5), 231.

London, D. (1986) Magmatic-hydrothermal transition in the Tanco rare-element pegmatite: evidence from fluid inclusions and phase-equilibrium experiments. Am. Mineral. 71, 376-395.

London, D. (1987) Internal differentiation of rare-element pegmatites: effects of boron, phosphorus, and fluorine. Geochim. Cosmochim. Acta. 51, 403-420.

Masuda, A. and Akagi, T. (1989) Lanthanide tetrad effect observed in leucogranites from China. Geochemical Journal, 23, 245-253.

Masuda, A. and Ikeuchi, Y. (1979) Lanthanide tetrad effect observed in marine environment. Geochem. J. 13, 19-22.

Masuda, A., Kawakami, O., Dohmoto, Y., Takenaka, T. (1987) Lanthanide tetrad effects in nature: two mutually opposite types, W and M. Geochemical Journal, 21, 119-124.

McLennan, S. M. (1994) Rare earth element geochemistry and the “tetrad” effect. Geochimica et Cosmochimica Acta, 58(9), 2025-2033.

Menzies, M. and Murthy, V. R. (1980) Mantle metasomatism as a precursor to the genesis of alkaline magmas: isotopic evidence. American Journal OF Science. 280A, 622-638.

Miyawaki, R., Matsubara, S., Yokohama, K., Takeuchi, K., Terada, Y., Nakai, I. (2000) Kozoite-(Nd), Nd(CO3)(OH), a new mineral in an alkali olivine basalt from Hizen-cho, Saga Prefecture, Japan. American Mineralogist, 85, 1076-1081.

Miyawaki, R., Matsubara, S., Yokohama, K., Iwano, S., Hamasaki, K., Yukinori, I. (2003) Kozoite-(La), $La(CO_3)(OH)$, a new mineral from Mitsukoshi, Hizen-cho, Saga Prefecture, Japan. Journal of Mineralogical and Petrological Sciences, 98, 137-141.

Monecke, T., Kempe, U., Monecke, J., Sala, M., Wolf, D. (2002) Tetrad effect in rare earth element distribution patterns: A method of quantification with application to rock and mineral samples from granite-related rare metal deposits. Geochimica et Cosmochimica Acta, 66(7), 1185-1196.

Möller, P. (1988) The dependence of partition coefficients on differences of ionic volumes in crystal-melt systems. Contrib. Mineral. Petrol. 99, 62-69.

Nagashima, K., Miyawaki, R., Takase, J., Nakai, I., Sakura, K., Matsubara, S., Kato, A., Iwano, S. (1986) Kimuraite, CaY2(CO3)4•6H2O, a new mineral from fissures in an alkali olivine basalt from Saga Prefecture, Japan, a new data on lokkaite. American Mineralogist, 71, 1028-1033.

Nakamura, E., Campbell, I. H. and Sun, S. S. (1985) The influence of subduction processes on the geochemistry of Japanese alkaline basalts. Nature. 316,55-58.

Nakamura, E., Campbell, I. H., McCulloch, M. T. and Sun, S. S. (1989) Chemical geodynamics in a back-arc region around the Sea of Japan: implications for the genesis of alkaline basalts in Japan, Korea and China. J. Geophys. Res. 94, 4634-4654.

Nakamura, E., McCulloch, M. and Campell, I. H. (1990) Chemical geodynamics in the back-arc region of Japan based on the trace element and Sr-Nd isotopic compositions. Tectonophysics. 174, 207-233.

Negro, D.A., Rossi, G. and Tazzoli, V. (1977) The crystal structure of lanthanite. *Am. Mineral.* 62.142-146.

Nugent, L. J., Baybarz, R. D., Burnett, J. L., Ryan, J. L. (1973) Electron-transfer and f-d absorption bands of some lanthanide and actinide complexes and the standard (II-III) oxidation potential for each member of the lanthanide and actinide series. J. Phys. Chem. 77, 1528-1539.

Ohta, A. and Kawabe, I. (2000) Theoretical study of tetrad effects observed in REE distribution coefficients between marine Fe-Mn deposit and deep seawater, and in REE(III)-carbonate complexation constants. Geochemical Journal, 34, 455-473.

Pearce, J. A., Baker, P. E., Harvey, P. K. and Luff, I. W. (1995) Geochemical evidence for subduction fluxes, mantle melting and fractional crystallization beneath the South Sandwich Island Arc. J. Petrology. 36(4), 1073-1109.

Peppard, D. F., Mason, G. W. and Lewey, S. (1969) A tetrad effect in the liquid-liquid extraction ordering of lanthanides (III). J. inorg. nucl. Chem., 31, 2271-2272.

Perttunen, V. (1971) Lokkaite, a new hydrous RE-carbonate from Pydriinmaa pegmatite in Kangasala, SW-Finland. Geological Society of Finland Bulletin. 43, 6l-72.

Ponader, C. W. and Gordon, E. B. (1989) Rare earth elements in silicate systems: II. Interactions of La, Gd, and Yb with halogens. Geochimica et Cosmochimica Acta. 53(11), 2905-2914.

Prouteau, G., Scaillet, B., Pichavant, M. and Maury, R. (2001) Evidence for mantle metasomatism by hydrous silicic melts derived from subducted oceanic crust. Nature. 410, 197-200.

Reisfeld, R. and Jørgensen, C. K. (1977) Lasers and Exited States of Rare Earths, Springer-Verlag, Berlin, 226.

Rizkalla, E. N. and Choppin, G. R. (1991) Hydration and hydrolysis of lanthanides. Handbook on the physics and chemistry of rare earths (Gschneidner, K. A., Jr. and Eyring, L., eds.). vol. 15, 393-442.

Rudnick, R. L., McDonough, W. F. and Chappell, B. W. (1993) Carbonatite metasomatism in the northern Tanzanian mantle: petrographic and geochemical characteristics. Earth and Planetary

Science Letters. 114, 463-475.

Seredin, V. V., Kremenetskii, A. A., Trach, G. N., Tomson, I. N. (2009) Doklady Earth Sciences, 425A(3), 403-408.

Shannon, R. D. (1976) Revised effective ionic radii and systematic studies of interatomic distances in halides and chalcogenides. Acta Cryst. 32, 751-767.

Takahashi, T., Tanaka, K. and Kawabe, I. (2007) Lanthanide tetrad effect of Naegi granite-pegmatite suite, central Japan: Convex tetrad effect by fractional loss of fluid from hydrous felsic melt. J. Earth planet. Sci. Nagoya Univ., 54, 13-35.

Takahashi, Y., Yoshida, H., Sato, N., Hama, K., Yusa, Y. and Shimisu, H. (2002) W- and M-type tetrad effects in REE patterns for water-rock system in the Tono uranium deposit, central Japan. Chemical Geology, 184, 311-335.

Tatsumoto, M., Basu, A. R., Huang, W. K., Wang, J. W. and Xie, G. H. (1992) Sr, Nd and Pb isotopes of ultramafic xenoliths in volcanic rocks of eastern China: enriched components EM Ⅰ and EM Ⅱ in sub-continental lithosphere. Earth Planet. Sci. Lett. 113, 107-128.

Taylor, S. R. and McLennan, S. M. (1985) The continental crust: Its composition and evolution. Blackwell, Oxford.

Tchougreeff, A. L. and Dronskowski, R. (2009) Nephelauxetic Effect Revisited. International Journal of Quantum Chemistry. 109, 2606-2621.

Uto, K. and Tatsumi, Y. (1996) Quaternary volcanism of the Japanese Islands. Island Arc. 5(3), 250-261.

Uto, K., Takahashi, E., Nakamura, E. and Kaneoka, I. (1994) Geochronology of alkali volcanism in Oki-Dogo Island, Southwest Japan: Geochemical evolution of basalts related to the opening of the Japan Sea Geochemical Journal. 28 (6), 431-449.

Vander Slius, K. L. and Nugent, L. J. (1972) Relative energies of the lowest levels of the $f^n ps^2$, $f^n ds^2$, and $f^{n+1}s^2$ electron configuration of the lanthanide and actinide neutral atoms. Phys. Rev. A6, 86-94.

Veksler, I. V., Dorfman, A. M., Kamenetsky, M., Dulski, P., Dingwell, D. B. (2005) Partitioning of lanthanides and Y between immiscible silicate and fluoride melts, fluorite and cryolite and the origin of the lanthanide tetrad effect in igneous rocks. Geochimica et Cosmochimica Acta, 69(11), 2847-2860.

Vorma, A., Ojanperä, P., Hoffrén, V., Siivola, J., Löfgren, A. (1966) Rare earth minerals from the Pyörönmaa pegmatite in Kangasala, southeastern Finland. Bulletin Commission Géologique de Finlande, 38,241-274.

Wass, S. Y., Henderson, P. and Elliott, C. J. (1980) Chemical heterogeneity and metasomatism in the upper mantle: evidence from rare earth and other elements in apatite-rich xenoliths in basaltic rocks from eastern Australia. Phil. Trans. R. Soc. Lond. A 297, 333-346.

Wass, S. Y. and Rogers, N. W. (1980) Mantle metasomatism-precursor to continental alkaline volcanism. Geochimica. et Cosmochimica. Acta. 44, 1811-1823.

Yanagi, T. and Maeda, S. (1998) Magma evolution observed in the Matsuura basalts in northwest Kyushu, Japan: An example of high-pressure open system fractional crystallization in a refilled magma chamber near the crust–mantle boundary. Physics of the Earth and Planetary Interiors, 107, 203-219.

Zhang, Z. C., Feng, C. Y., Li, Z. N., Li, S. C., Xin, Y., Li, Z. M. and Wang, X. Z. (2002) Petrochemical study of the Jingpohu Holocene alkali basaltic rocks, Northeastern China. Geochemical Journal. 36, 133-153.

Acknowledgement

This research project would not have been possible without the support of many people, and I would like to express my gratitude to all those who gave me the possibility to complete this thesis.

In the first instance, I wish to express my love and gratitude to my beloved families, my father, my mother and all members, not only for their material support, but also for their understanding and endless love, which have sustained me through the entire duration of my studies. Especially, I would like to give my sincere appreciation to Kai Zhou whose vast patience and love enabled me to complete this thesis.

I owe my deepest gratitude to my supervisor Prof. Kawabe Iwao. His instructions, stimulating suggestions and encouragement helped me in all the time of my research and my writing of this thesis. At the same time, his knowledge and kind advices have been of great helpful to my daily life in Japan.

I am deeply indebted to my former colleagues, including Prof. Yuanbao Wu, Prof. Yongsheng Liu, Assistant Rui Liu, Assistant Hua Xiang, Doc. Song Jin, Doc. Saihong Yang, Min Peng, Jing Wang and Xiochi Liu. They led me to the geochemistry world, and encouraged me to take the opportunity to study abroad. In my difficult times, their constructive suggestions, valuable hints and support were very helpful.

I have furthermore to express my thanks to the present colleagues in geochemistry office, Prof. Tanaka, Prof. Tsuyoshi Yamamoto, Associate Prof. Koichi Mimura, Associate Prof. Yasuhiro Hirahara, Assistant Prof. Yoshihiro Asahara and Secretary Yumi Sasaki. They always show deep concerns about my research and my living in Japan, and make their supports available in a number of ways.

Especially I am obliged to Prof. Yamamoto Tsuyoshi, as his assistance of ICP-MS analysis is an indispensable part of my thesis. Meanwhile, special thanks also to Assistant Prof. Takenori Kato, who assisted with the EPMA analysis, and reviewed my manuscript. It is an honor for me to express my sincere appreciation to Tetsuo Minagawa, as the kimuraite sample used in our study is donated by him. I also want to thank Doctor Kazuya Miyagawa, Doctor Kazuhiro Suzuki and Doctor Haruna Sugahara, for all their concerns, help, encouragement and advice.

I would like to show my gratitude to all the students, who were and are in this office. They have created a bright and cheerful atmosphere to back up my research. And it is my big pleasure to thank those who made creative discussions and gave

critical comments on my study in the anniversary meeting.

I am also grateful to the editorial members of Chemical Geology, American Mineralogist, Canadian Mineralogist and Geochemical Journal, as well as the anonymous reviewers. Their critical suggestions and unique point of view made enormous contributions to my papers. I also feel thankful to all my friends, who always stand by my side. Every time I contact with them, I get power and courage to go ahead.

In the end, I would like to thank all people who directly and indirectly provide assistance for my study.